Glial cell-derived neuroregulators control type 3 innate lymphoid cells and gut defence

Sales Ibiza[#1], **Bethania García-Cassani**[#1], **Hélder Ribeiro**[1], **Tânia Carvalho**[1], **Luís Almeida**[1], **Rute Marques**[2,†], **Ana M. Misic**[3,‡], **Casey Bartow-McKenney**[3], **Denise M. Larson**[4], **William J. Pavan**[4], **Gérard Eberl**[2], **Elizabeth A. Grice**[3], and **Henrique Veiga-Fernandes**[1,5]

[1]Instituto de Medicina Molecular, Faculdade de Medicina de Lisboa, Av. Prof. Egas Moniz, Edifício Egas Moniz, 1649-028 Lisboa, Portugal

[2]Microenvironment and Immunity Unit, Institut Pasteur, 25 Rue du Docteur Roux, 75724 Paris, France

[3]Department of Dermatology, Perelman School of Medicine, University of Pennsylvania, 421 Curie Blvd, 1007 Biomedical Research Building, Philadelphia, PA 19104, US

[4]Genetic Disease Research Branch, National Human Genome Research Institute, National Institutes of Health, Bethesda, MD 20892, US

[5]Champalimaud Research. Champalimaud Centre for the Unknown. 1400-038 Lisbon, Portugal

[#] These authors contributed equally to this work.

Abstract

Group 3 innate lymphoid cells (ILC3) are major regulators of inflammation and infection at mucosal barriers1. ILC3 development has been considered to be programmed1. Nevertheless, how ILC3 perceive, integrate and respond to local environmental signals remains unclear. Here we show that ILC3 sense their environment and control gut defence as part of a novel glial-ILC3-epithelial cell unit orchestrated by neurotrophic factors. We found that enteric ILC3 express the neuroregulatory receptor RET. ILC3-autonomous *Ret* ablation led to decreased innate interleukin-22 (IL-22), impaired epithelial reactivity, dysbiosis and increased susceptibility to bowel inflammation and infection. Neurotrophic factors directly controlled innate *Il22,* downstream of p38 MAPK/ERK-AKT cascade and STAT3 activation. Strikingly, ILC3 were

adjacent to neurotrophic factor expressing glial cells that exhibited stellate-shaped projections into ILC3 aggregates. Glial cells sensed microenvironmental cues in a MYD88 dependent manner to control neurotrophic factors and innate IL-22. Accordingly, glial-intrinsic *Myd88* deletion led to impaired ILC3-derived IL-22 and pronounced propensity to gut inflammation and infection. Our work sheds light into a novel multi-tissue defence unit, revealing glial cells as central hubs of neuron and innate immune regulation via neurotrophic factor signals.

Group 3 innate lymphoid cells (ILC3) produce pro-inflammatory cytokines, regulate mucosal homeostasis and anti-microbial defence[1]. In addition to their well-established developmentally regulated program, ILC3 are also controlled by microbial and dietary signals[1–6] raising the hypothesis that ILC3 possess other unexpected environmental sensing strategies. Neurotrophic factors are extra-cellular environmental cues to neurons and include the glial-derived neurotrophic factor (GDNF) family ligands (GFL) that activate the tyrosine kinase receptor RET in the nervous system, kidney and haematopoietic progenitors[7–11].

Analysis of gut lamina propria revealed that ILC3 express high levels of *Ret* (Fig.1a)[7,12], a finding confirmed at the protein level and by *Ret*[GFP] knock-in mice (Fig.1b-d and Extended Data Fig.1a-d)[13]. ILC3 subsets expressed *Ret*[GFP] and aggregated in Cryptopatches (CP) and Isolated Lymphoid Follicles (ILF), suggesting a role of neuroregulators in ILC3 (Fig.1b-d and Extended Data Fig.1b-j). To explore this hypothesis, we transplanted foetal liver cells from *Ret* competent (*Ret*[WT/GFP]) or deficient (*Ret*[GFP/GFP])[13] animals into alymphoid *Rag1*^{-/-} *Yc*^{-/-} hosts. *Ret* deficient chimeras revealed unperturbed ILC3 and CP development (Fig.1e). Strikingly, IL-22 expressing ILC3 were largely reduced despite normal IL-22 producing T cells (Fig.1f,g). In contrast, innate IL-17 was unaffected by *Ret* ablation (Fig.1f and Extended Data Fig.2a). In agreement, analysis of gain-of-function *Ret*[MEN2B] mice[14] revealed a selective increase of IL-22 producing ILC3 while their IL-17 counterparts were unaffected (Fig.1h and Extended Data Fig.2b). To more specifically evaluate the effects of RET in ILC3, we deleted *Ret* in RORγt expressing cells by breeding *Rorgt*-Cre to *Ret*^{fl/fl} mice[15,16] (Extended Data Fig.3a,b). Analysis of *Rorgt*-Cre.*Ret*^{fl/fl} (*Ret*) mice revealed selective and large reduction of ILC3-derived IL-22, but normal IL-22 producing T cells (Fig.2a and Extended Data Fig.3c,d). IL-22 acts on epithelial cells to induce reactivity and repair genes[1]. When compared to their wild-type (WT) littermate controls, the *Ret* epithelium revealed normal morphology, proliferation and paracellular permeability, but a profound reduction of epithelial reactivity and repair genes (Fig.2b and Extended Data Fig. 3e-h). Accordingly, the *Ret*[MEN2B] epithelium displayed increased levels of these molecules in an IL-22 dependent manner (Fig.2b and Extended data Fig.3i). These results indicate that RET signals selectively control innate IL-22 and shape intestinal epithelial reactivity.

To interrogate whether neurotrophic factors regulate intestinal defence we tested how varying degrees of RET signals control enteric aggressions. While *Ret* mice treated with Dextran Sodium Sulfate (DSS) had increased weight loss and inflammation, reduced IL-22 producing ILC3, decreased epithelial reactivity/repair genes and pronounced bacterial translocation from the gut, *Ret*[MEN2B] mutants were highly protected over their WT littermate controls (Fig.2c-j and Extended Data Fig.4). Since DSS mostly causes epithelial injury, we tested whether ILC3-autonomous RET signals are required to control infection.

To this end, *Ret* mice were bred to *Rag1*^{-/-} mice to formally exclude adaptive T cell effects. *Rag1*^{-/-}.*Ret* mice were infected with the attaching and effacing bacteria *Citrobacter rodentium*. When compared to their littermate controls, *Rag1*^{-/-}.*Ret* mice had marked gut inflammation, reduced IL-22 producing ILC3, increased *C. rodentium* infection and translocation, reduced epithelial reactivity genes, increased weight loss and reduced survival (Fig.2k-n and Extended Data Fig.5). Altogether, these data indicate that ILC3-intrinsic neurotrophic factor cues regulate gut defence and homeostasis.

Formal definition that IL-22 is the molecular link between RET-dependent ILC3 activation and epithelial reactivity was provided by a multi-tissue organoid system. Addition of GFL to ILC3/epithelial organoids strongly induced epithelial reactivity genes in an IL-22 and RET dependent manner (Fig.3a,b and Extended Data Fig.6a). To further examine how RET signals control innate IL-22 we investigated a gene signature associated with ILC identity[1]. While most of those genes were unperturbed, notably the master ILC transcription factors *Runx1, Id2, Gata3, Rora, Rorgt, Ahr and Stat3*, *Il22* was significantly reduced in *Ret* ILC3 (Fig.3c and Extended Data Fig.6b). In agreement, activation of ILC3 with all or distinct GFL/GFRα pairs *in trans* efficiently increased *Il22* despite normal expression of other ILC3-related genes (Fig.3d and Extended Data Fig.6c). Activation of RET by GFL leads to p38 MAPK/ERK-AKT cascade activation in neurons, while phosphorylation of STAT3 shapes *Il22* expression[7,17]. Analysis of *Ret* ILC3 revealed hypo-phosphorylated ERK1/2, AKT, p38/MAP kinase and STAT3 (Fig.3e and Extended Data Fig.6d). Accordingly, GFL-induced RET activation in ILC3 led to rapid ERK1/2, AKT, p38/MAP kinase and STAT3 phosphorylation and increased *Il22* transcription (Fig.3d,f and Extended Data Fig.6e,f). In agreement, inhibition of ERK, AKT or p38/MAP kinase upon GFL activation led to impaired STAT3 activation and *Il22* expression (Fig.3g,h). Finally, inhibition of STAT3 upon GFL-induced RET activation led to decreased *Il22* (Fig.3h). To examine whether GFL directly regulate *Il22* we performed chromatin immunoprecipitation (ChIP) (Fig.3i,j)[18]. Stimulation of ILC3 with GFL resulted in increased binding of pSTAT3 in the *Il22* promoter and increased trimethyl-H3K36 at the 3' end of *Il22,* indicating active *Il22* transcribed regions (Fig.3d,j)[19]. Thus, cell-autonomous RET signals control ILC3 function and gut defence via direct regulation of *Il22* downstream of STAT3 activation.

Propensity to inflammation and dysregulation of intestinal homeostasis have been associated to dysbiosis[20,21]. When compared to their WT littermates, *Ret* mice have altered microbial communities as evidenced by quantitative analysis, weighted UniFrac analysis and significantly altered levels of *Sutterella*, unclassified *Clostridiales* and *Bacteroides* (Fig.4a and Extended Data Fig.7). Discrete microbial communities may have transmissible colitogenic potential[20,21]. Nevertheless, germ-free mice colonised with the microbiota of *Ret* or their control littermates revealed similar susceptibility to DSS-induced colitis and identical innate IL-22 (Fig.4b-d). In agreement, co-housed *Ret* and WT littermates had differential propensity to intestinal inflammation (Fig.2c,d). Together, these data indicate that dysbiosis *per se* is insufficient to cause altered innate IL-22 and susceptibility to gut inflammation as observed in *Ret* mice (Fig.2c-f). Thus, we hypothesised that GFL producing cells integrate commensal and environmental signals to control innate IL-22. Accordingly, antibiotic treatment of *Ret* and their WT littermate controls resulted in similar ILC3-derived IL-22 (Fig.4e)[22].

Neurotrophic factors of the GDNF family were shown to be produced by enteric glial cells, which are neuron-satellites expressing the glial fibrillary acidic protein (GFAP)[7,23]. Strikingly, double reporter mice for ILC3 (Ret^{GFP}) and glial cells ($Gfap$-Cre.$Rosa26^{RFP}$) revealed that stellate-shaped projections of glial cells are adjacent (4.35μm±1.42) to RORγt⁺ ILC3 within CP (Fig.4f and Extended Data Fig.8a). These data suggest a paracrine glial-ILC3 crosstalk orchestrated by neurotrophic factors. In agreement, lamina propria glial cells were main producers of GFL (Extended Data Fig.8b). Recent studies have shown that glial cells express pattern recognition receptors, notably Toll-like receptors (TLRs)[24,25]. Activation of neurosphere-derived glial cells revealed they specifically respond to TLR2, TLR4, and the alarmins IL-1β and IL-33, which efficiently controlled GFL expression and induced robust innate *Il22* in a MYD88 dependent manner (Fig.4g-i and Extended Data Fig. 8c-g). To formally demonstrate the physiological importance of MYD88-dependent glial cell sensing on innate IL-22, we deleted *Myd88* in GFAP expressing glial cells by breeding *Gfap*-Cre to *Myd88*^fl/fl mice[26,27]. Remarkably, glial-intrinsic deletion of *Myd88* resulted in decreased intestinal GFL, increased gut inflammation, impaired ILC3-derived IL-22, and increased weight loss (Fig.4j-m; Extended Data Fig.9a-d). In agreement, *Gfap*-Cre.*Myd88* mice had increased susceptible to *C.rodentium* infection (Extended Data Fig.9e-h). Thus, mucosal glial cells orchestrate innate IL-22 via neurotrophic factors, downstream of MYD88-dependent sensing of commensal products and alarmins.

Defining the mechanisms by which ILC3 integrate environmental cues is critical to understand mucosal homeostasis. Our work sheds light on the relationships between ILC3 and their microenvironment, notably through decoding a novel glial-ILC3-epithelial cell unit orchestrated by neurotrophic factors (Extended Data Fig.10). Glial-derived neurotrophic factors operate in an ILC3-intrinsic manner by activating the tyrosine kinase RET, which directly regulates innate IL-22 downstream of p38 MAPK/ERK-AKT and STAT3 phosphorylation (Extended Data Fig.10). Future studies will elucidate further the mechanisms inducing RET expression in ILC3.

Our data demonstrate that in addition to their well-established capacity to integrate dendritic cell-derived cytokines[1], ILC3 perceive distinct multi-tissue regulatory signals leading to STAT3 activity and IL-22 expression, notably via integration of glial cell-derived neuroregulators. Thus, rather than providing hard-wired signals for ILC3-immunity, we propose that RET signals critically fine-tune innate IL-22 leading to efficient gut homeostasis and defence.

Previous studies demonstrated that neurons can indirectly shape foetal lymphoid tissue inducer cells and that ablation of glial cells leads to gut inflammation[28,29]; here we reveal glial cells as central hubs of neuronal and innate immune regulation. Notably, neurotrophic factors are the molecular link between glial cell sensing, innate IL-22 and intestinal epithelial defence. Thus, it is tempting to speculate that glial/immune cell units might be also critical to the homeostasis of other barriers, notably in the skin, lung and brain[30]. From an evolutionary perspective, coordination of innate immunity and neuronal function may ensure efficient mucosal homeostasis and a co-regulated neuro-immune response to various environmental challenges, including xenobiotics, intestinal infection, dietary aggressions and cancer.

Methods

Mice

C57BL/6J mice were purchased from Charles River. Ret^{GFP} 13, $Rag1^{-/-}\gamma c^{-/-}$ 31,32, Ret^{MEN2B} 14, $Rosa26^{YFP}$ 33, $Rosa26^{RFP}$ 34, $Ret^{fl/fl}$ 16, $Rorgt$-Cre 15, $Il1b^{-/-}$ 35 and $Myd88^{-/-}$ 36 were in a full C57BL/6J background. $Gfap$-Cre26 bred to $Myd88^{fl/fl}$ 27 were in F8-F9 to a C57Bl/6J background. All lines were bred and maintained at IMM Lisboa animal facility. Mice were systematically compared with co-housed littermate controls. Both males and females were used in this study. Randomization and blinding were not used unless stated otherwise. All animal experiments were approved by national and institutional ethical committees, respectively Direção Geral de Veterinária and iMM Lisboa ethical committee. Germ-free mice were housed at Instituto Gulbenkian de Ciência, Portugal, and Institut Pasteur, France, in accordance to institutional guidelines for animal care. Power analysis was performed to estimate the number of experimental mice.

Generation of foetal liver chimeras

For reconstitution experiments, 5×10^6 foetal liver cells were isolated from E14.5 $Ret^{WT/GFP}$ or $Ret^{GFP/GFP}$ mice and injected intravenously into non-lethally irradiated (200rad) alymphoid $Rag1^{-/-}\gamma c^{-/-}$ hosts. Mice were analysed 8 weeks post-transplantation.

Dextran Sodium Sulphate-induced colitis

Dextran Sodium Sulphate (DSS) (molecular mass 36,000-50,000 Da; MP Biomedicals) was added into drinking water 3% (w/v) for 5 days followed by 2 days of regular water. Mice were analysed at day 7. Body weight, presence of blood and stool consistency was assessed daily.

Citrobacter rodentium infection

Infection with *Citrobacter rodentium* ICC180 (derived from DBS100 strain)37 was performed by gavage inoculation of 10^9 colony forming units37,38. Acquisition and quantification of luciferase signal was performed in an IVIS system (Caliper Life Sciences). Throughout infection, weight loss, diarrhoea and bloody stools were monitored daily.

Antibiotic treatment

Pregnant females or new born mice were treated with streptomycin 5g/L, ampicillin 1g/L and colistin 1g/L (Sigma-Aldrich) into drinking water with 3% sucrose. Control mice were given 3% sucrose in drinking water as previously described22.

Microscopy

Intestines from Ret^{GFP} and Ret^{GFP} chimeras were imaged in a Zeiss Lumar V12 fluorescence stereo microscope with a NeoLumar S 0.8x objective using the GFP filter. Whole-mount analysis was performed as previously described2,9. Briefly, adult intestines were flushed with cold PBS (Gibco) and opened longitudinally. Mucus and epithelium was removed and intestines were fixed in 4% PFA (Sigma-Aldrich) at room temperature for 10 minutes and incubated in blocking/permeabilising buffer solution (PBS containing 2% BSA,

2% goat serum, 0.6% Triton X-100). To visualise three-dimensional structures of the small intestine, samples were cleared with benzyl alcohol-benzyl benzoate (Sigma-Aldrich) prior dehydration in methanol[2,9]. For analysis of thick gut sections intestines were fixed with 4% PFA at 4°C overnight and were then included in 4% low-melting temperature agarose (Invitrogen). Sections of 100μm were obtained with a Leica VT1200/VT1200 S vibratome and embedded in Mowiol (Calbiochem)[2]. Slides or whole-mount samples were incubated overnight or for 1–2 days respectively at 4°C using the following antibodies: rat monoclonal anti-B220 (RA3-6B2) (eBioscience), mouse monoclonal anti-RORγt (Q31-378) (BD Pharmigen), mouse monoclonal anti-GFAP (GA-5) (Sigma-Aldrich), mouse monoclonal anti-GFAP Cy3 (GA-5) (Abcam), anti-GDNF antibody (Abcam), DAPI (4',6-Diamidino-2-Phenylindole, Dihydrochloride) (Invitrogen). A647 goat anti-rat, A568 goat anti-rat, A647 goat anti-mouse, A488 rabbit anti-GFP, and A488 goat anti-rabbit secondary antibodies were purchased from Invitrogen. Neurospheres and cultured glial cells were fixed in PFA 4% 10 minutes at room temperature and permeabilised in PBS-Triton 0.1% during 30 seconds. After several washing steps with PBS cells were incubated with antibodies during 3h at room temperature and then mounted in Mowiol[39]. Samples were acquired on a Zeiss LSM710 confocal microscope using EC Plan-Neofluar 10x/0.30 M27, Plan Apochromat 20x/0.8 M27 and EC Plan-Neofluar 40x/1.30 objectives. Three-dimensional reconstruction of images was achieved using Imaris software and snapshot pictures were obtained from the three-dimensional images. For analysis of confocal images, cells were counted using in-house software, written in MATLAB (Mathworks, Natick, MA). Briefly, single-cell ILC3 nuclei were identified via RORγt by thresholding and particle analysis. Regions of interest (ROIs) (Extended Data Fig.1i; Bottom panels) were defined from each nucleus for analysis in the GFP channel, where staining was considered positive if a minimum number of pixels (usually 20) were above a given threshold. The software allows for batch processing of multiple images and generates individual report images for user verification of cell-counting results and co-expression analysis: (https://imm.medicina.ulisboa.pt/en/servicos-e-recursos/technical-facilities/bioimaging).

Histopathology analysis

Colon samples were fixed in 10% neutral buffered formalin. The colon was prepared in multiple cross-sections or "Swiss roll" technique[40], routine-processed for paraffin embedding and 3-4μm sections were stained with haematoxylin and eosin. Enteric lesions were scored by a pathologist blinded to experimental groups, according to previously published criteria[41–43]. Briefly, lesions were individually scored (0-4 increasing severity) for the following criteria: 1-mucosal loss; 2-mucosal epithelial hyperplasia, 3-degree of inflammation, 4-extent of the section affected in any manner and 5-extent of the section affected in the most severe manner as previously described[43]. Final scores were derived by summing the individual lesion and the extent scores. The internal diameter of the crypts was measured in at least five fields (10x magnification), corresponding to the hotspots in which the most severe changes in crypt architecture were seen. Measurements were performed in an average of 35 crypts per sample/mouse, from proximal to distal colon. Intestinal villus height was measured in the jejunum. Measurements were performed in slides scanned using a Hamamatsu Nanozoomer SQ digital slide scanner running NDP Scan software.

Enteric glial cell isolation

Enteric glial cells isolation was adapted from previously described protocols[44,45]. Briefly, the muscularis layer was separated from the submucosa with surgical forceps under a dissection microscope (SteREO Lumar.V12, Zeiss). The lamina propria was scraped mechanically from the underlying submucosa using 1.5mm cover-slips (Thermo Scientific). Isolated tissues were collected and digested with Liberase TM (7,5 μg/mL; Roche) and DNase I (0.1mg/ mL; Roche) in RPMI supplemented with 1% hepes, sodium pyruvate, glutamine, streptomycin and penicillin and 0.1% β-mercaptoethanol (Gibco) for approximately 40min at 37°C. Single-cell suspensions were passed through a 100μm cell strainer (BD Biosciences) to eliminate clumps and debris.

Flow cytometry and cell sorting

Lamina propria cells were isolated as previously described[46]. Briefly, intestines were digested with collagenase D (0.5mg/mL; Roche) and DNase I (0.1 mg/ mL; Roche) in RPMI supplemented with 10% FBS, 1% hepes, sodium pyruvate, glutamine, streptomycin and penicillin and 0.1% β-mercaptoethanol (Gibco) for approximately 30min at 37°C under gentle agitation. For cytokine analysis, cell suspensions were incubated 4h in PMA/ Ionomycin (Sigma-Aldrich) and Brefeldin A (eBioscience) at 37ºC. Intracellular staining was performed using IC fixation/permeabilisation kit (eBioscience). Cells were stained using PBS, 1% FBS, 1% hepes and 0.6% EDTA (Gibco). Flow cytometry analysis and cell sorting were performed using FORTESSA and FACSAria flow cytometers (BD Biosciences). Data analysis was done using FlowJo software (Tristar). Sorted populations were >95% pure. Cell suspensions were stained with anti-CD45 (30-F11), anti-TER119 (TER-119), TCRβ (H57-597), anti-CD3ε (eBio500A2), anti-CD19 (eBio1D3), anti-NK1.1 (PK136), anti-CD11c (N418), anti-Gr1 (RB6-8C5), anti-CD11b (Mi/70), anti-CCR6 (29-2L17), anti-CD127 (IL-7Rα; A7R34), anti-Thy1.2 (53-2.1), anti-CD49b (DX5), anti-TCRδ (GL3), anti-NKp46 (29A1.4), anti-IL-17 (eBio17B7), anti-IL-22 (1H8PWSR), Rat IgG1 isotype control (eBRG1) antibodies, 7AAD viability dye, anti-Mouse CD16/CD32 (Fc block), anti-RORγt (AFKJS-9); Rat IgG2a$_k$ Isotype Control (eBR2a) and streptavidin fluorochrome conjugates all from eBioscience; anti-CD4 (GK1.5), anti-CD31 (390), anti-CD8α (53-6.7), anti-CD24 (M1/69), anti-Epcam (G8.8) antibodies were purchased from Biolegend. Anti-RET (IC718A) antibody was purchased from R&D Systems. LIVE/DEAD Fixable Aqua Dead Cell Stain Kit was purchased from Invitrogen. Cell populations were defined as: ILC3 - CD45+Lin-Thy1.2hiIL7Rα+RORγt+; For ILC3 subsets additional markers were employed: LTi - CCR6+Nkp46-; ILC3 NCR- - CCR6-Nkp46-; ILC3 NCR+ - CCR6-Nkp46+; Lineage was composed by CD3ε, CD8α, TCRβ, TCRγδ, CD19, Gr1, CD11c and TER119; Glial cells - CD45-CD31-TER119-CD49b+ [47]; T cells - CD45+CD3ε+; γδ T cells - CD45+CD3ε+γδTCR+; B cells - CD45+CD19+B220+; Macrophages - CD45+CD11b+F4/80+; Dendritic cells - CD45+CD19-CD3ε-MHCII+CD11c+; enteric neurons - CD45-RET/GFP+ [13], Epithelial cells - CD45-CD24+Epcam+.

Quantitative RT-PCR

Total RNA was extracted using RNeasy micro kit (Qiagen) or Trizol (Invitrogen) according to the manufacturer's protocol. RNA concentration was determined using Nanodrop

Spectrophotometer (Nanodrop Technologies). Quantitative real-time RT–PCR was performed as previously described2,8,9. *Hprt* and *Gapdh* were used as housekeeping genes. For TaqMan assays (Applied Biosystems) RNA was retro-transcribed using a High Capacity RNA-to-cDNA Kit (Applied Biosystems), followed by a pre-amplification PCR using TaqMan PreAmp Master Mix (Applied Biosystems). TaqMan Gene Expression Master Mix (Applied Biosystems) was used in real-time PCR. TaqMan Gene Expression Assays (Applied Biosystems) were the following: *Gapdh* Mm99999915_g1; *Hprt* Mm00446968_m1; *Artn* Mm00507845_m1; *Nrtn* Mm03024002_m1; *Gdnf* Mm00599849_m1; *Gfra1 Mm00439086_m1; Gfra2 Mm00433584_m1; Gfra3 Mm00494589_m1; Ret* Mm00436304_m1; *Il22* Mm01226722_g1; *Il17a* Mm00439618_m1; *Il23r* Mm00519943_m1; *Rorgt* Mm01261022_m1; *Il7ra* Mm00434295_m1; *Ahr* Mm00478932_m1; *Stat3* Mm01219775_m1; *Cxcr6* Mm02620517_s1; *Nfkbiz* Mm_00600522_m1; *RegIIIa* Mm01181787_m1; *RegIIIb* Mm00440616_g1; *RegIIIg* Mm00441127_m1; *Defa1* Mm02524428_g1; *Defa-rs1* Mm00655850_m1; *Defa5* Mm00651548_g1; *Defa21* Mm04206099_gH; *Muc1* Mm00449599_m1; *Muc3* Mm01207064_m1; *Muc13* Mm00495397_m1; *Gfap* Mm01253033_m1*; Ascl2* Mm01268891_g*; Tff3* Mm00495590_m1*; Relm-b* Mm00445845_m1*; Pla2g2a* Mm00448160_m1*; Pla2g5* Mm00448162_m1*; Wnt3* Mm00437336_m1*; Ctnnb1* Mm00483039_ m1*; Axin2* Mm00443610_m1*; Dll1b* Mm01279269_m1*; Il18* Mm00434225_m1*; Tnfa* Mm00443260_g1*; Lyz1* Mm00657323_m1*; Lrg5* Mm00438890_m1*; Tbx21* Mm00450960_m1*; Id2* Mm00711781_m1*; Runx1* Mm01213404_m1*; Notch1* Mm00435249_m1*; Notch2* Mm00803077_m1*; Gata3* Mm00484683_m1*; Bcl2* Mm00477631_m1*; Bcl2l1* Mm00437783_m1*; Arntl* Mm00500226_m1; *Glpr2* Mm01329475_m1; *Gja1* Mm01179639_s1; *Ednrb* Mm00432989; *S100b* Mm00485897_m1; *Sox10* Mm00569909_m1. Real-time PCR analysis was performed using ABI Prism 7900HT Sequence Detection System or StepOne Real-Time PCR system (Applied Biosystems).

ILC3 activation and cell signalling

Sorted intestinal ILC3 cells were starved for 3 hours in RPMI at 37°C in order to ensure ILC3 viability. *Ret*[l] or *Ret* were analysed directly *ex vivo*. To test ERK, AKT, p38-MAPK (Cell Signaling Technology) and STAT3 (BD Pharmigen) upon GFL stimulation WT ILC3 were activated with 500ng/mL (each GFL) and co-receptors (rrGFR-α1, rmGFR-α2, rrGFR-α3 and rrGNDF from R&D Systems; rhNRTN and rhARTN from PeproTech) for 10 and 30min. When referring to the use of 'GFL', we have employed GDNF, NRTN, ARTN and their specific co-receptors in combination. For inhibition experiments cells were incubated 1h at 37°C before GFL stimulation, to test ERK, AKT, p38/MAPK and STAT3 phosphorylation, or during overnight stimulation with GFLs, to determine *Il22* expression levels. Inhibitors were purchased from Sigma-Aldrich: p38 MAPK/ERK-AKT - LY294002 (LY); ERK - PD98059 (PD); AKT - AKT Inhibitor VIII (VIII); p38 MAPK - SB 202190 (SB); and pSTAT3 – S3I-201 (S3I).

Chromatin immunoprecipitation (ChIP) assay

Enteric ILC3 from adult C57BL/6J mice were isolated by flow cytometry. Cells were starved for 3h with RPMI supplemented with 1% hepes, sodium pyruvate, glutamine,

streptomycin and penicillin and 0.1% β-mercaptoethanol (Gibco) at 37°C. Cells were stimulated with GFLs (500ng/mL each)[8], lysed, cross-linked and chromosomal DNA-protein complex sonicated to generate DNA fragments ranging from 100-300 base pairs. DNA/protein complexes were immunoprecipitated, using LowCell# ChIP kit (Diagenode)[18], with 3μg of rabbit polyclonal antibody against anti-pSTAT3 (Cell Signalling Technology), rabbit control IgG (Abcam) or H3K36me3 (07-030; Millipore). Immunoprecipitates were uncross-linked and analysed by quantitative PCR using primer pairs (5'-3') flanking putative sites on *Il22*. Vehicle (BSA) stimulated ILC3s were used as controls. *Il22* primer sequences were previously described[48–50], briefly: a, F-TGCAATCAATCCCAGTATTTTG and R-CTTGTGCAAGCATAAGTCTCAA; b, F-GAAGTTGGTGGGAAAATGAGTCCGTGA and R-GCCATGGCTTTGCCGTAGTAGATTCTG; c, F-ACGGGAGATCAAAGGCTGCTCT and R-GCCAACAAGGTGCTTTTGC; d, F-CTCACCGTGACGTTTTAGGG and R-GTGAATGATATGACATCAGAC; e, F-CGACGAACATGCTCCCCTGATGTTTTT and R-AAACTCATAGATTTCTGCAGGACAGCC; f, F-AGCTGCATCTCTTTCTCTCCA and R-TATCCTGAAGGCCAAAATAGGA; g, F-ACGACCAGAACATCCAGAAGA and R-GCAGAGAAAGAAATCCCCGC; h, F-AGGGGGACTTGCTTTGCCATTT and R-AACACCCCTTCTTTCCTCCTCCAT; i, F-CTGCTCCTTCCTGCCTTCTA and R-CTGAGCCAGGTTTCATGTGA. Primer positions are shown in Fig.3i relative to the transcription start codon of *Il22*.

Colony forming units and paracellular permeability

Organs were harvested, weighed, and brought into suspension. Bacterial colony forming units (CFU) were determined per gram of tissue and total organ. CFU were determined via serial dilutions on Luria Broth (LB) agar and MacConkey agar (Sigma-Aldrich). Colonies were counted after 2 days of culture at 37ºC. To address intestinal paracellular permeability 16 mg per mouse of Dextran-Fitc (Sigma Aldrich) were administrated by gavage after overnight starvation. Plasma was analysed after 4 hours of Dextran-Fitc administration using a Microplate Reader TECAN Infinity F500.

BrdU administration and Ki-67 labeling

BrdU was administrated by i.p. injection (1.25 mg/mouse). For flow cytometric analysis of epithelial cell proliferation anti-BrdU (Staining Kit for flow Cytometry- eBioscience) and anti-mouse Ki-67 antibody (BioLegend) were employed.

Quantitative PCR analysis of bacteria in stool at the Phylum level

DNA from faecal pellet samples was isolated with ZR Fecal DNA MicroPrep™ (Zymo Research). Quantification of bacteria were determined from standard curves established by qPCR. qPCR were performed with Power SYBR® Green PCR Master Mix (Applied Biosystems) and different primer sets using a StepOne Plus (Applied Biosystems) thermocycler. Samples were normalized to 16S rDNA and reported according to the $2^{-\Delta CT}$ method. Primer sequences were: 16S rDNA, F- ACTCCTACGGGAGGCAGCAGT and R-ATTACCGCGGCTGCTGGC; *Firmicutes*, F- ACTCCTACGGGAGGCAGC and R-GCTTCTTAGTCAGGTACCGTCAT; *Bacteroidetes*, F- GGTTCTGAGAGGAGGTCCC and

R-GCTGGCTCCCGTAGGAGT; *Proteobacteria*, F- GGTTCTGAGAGGAGGTCCC and R-GCTGGCTCCCGTAGGAGT.

16S rRNA quantification and gene sequencing

Faeces were isolated from co-housed *Ret*^{fl} or *Ret* littermates. Sequencing of the 16S *rRNA* gene was performed as previously described[51]. Briefly, barcoded primers were used to amplify the V4 region of the 16S *rRNA* gene, and the amplicons were sequenced on a MiSeq instrument (Illumina, San Diego, USA) using 150 bp, paired-end chemistry at the University of Pennsylvania Next Generation Sequencing Core. The paired ends were assembled and quality filtered, selecting for reads with a quality score 30. Reads with >10 bp homopolymers and reads shorter than 248 bp or longer than 255 bp were removed from the analysis. 16S rRNA sequence data were processed using mothur v 1.25.0[52] and QIIME v 1.8[53]. Chimeric sequences were removed with ChimeraSlayer[54]. Operational taxonomic units (OTUs) were defined with CD-HIT[55] using 97% sequence similarity as a cut-off. Only OTUs containing 2 sequences were retained; OTUs assigned to Cyanobacteria or which were not assigned to any phylum were removed from the analysis. Taxonomy was assigned using the Ribosomal Database Project (RDP) classifier v 2.2[56], multiple sequence assignment was performed with PyNAST (v 1.2.2)[57], and FastTree[58] was used to build the phylogeny. Samples were rarified to 22,000 sequences per sample for alpha- and beta-diversity analyses. Taxonomic relative abundances are reported as the median with standard deviation. P values were calculated using the Wilcoxon rank-sum test. Statistical tests were conducted in R v. 3.2.0. To determine which factors were associated with microbial community composition, statistical tests were performed using the non-parametric analysis of similarities (ANOSIM) with weighted UniFrac distance metrics[59].

Data accession

The sequencing data generated in this study have been submitted to the NCBI Sequence Read Archive under BioProject PRJNA314493 (SRA: http://www.ncbi.nlm.nih.gov/sra/?term=PRJNA314493).

Intestinal organoids

IntestiCult™ Organoid Growth Medium and Gentle Cell Dissociation Reagent were purchased from StemCell. Intestinal crypts were isolated from C57BL/6J mice according to the manufacturer's instructions and were added to previously thawed, ice-cold Matrigel at a 1:1 ratio and at a final concentration of 5,000-7,000 crypts/mL. 15μL of this mix was plated per well of a 96 well round-bottom plate. After Matrigel solidification 100μL of growth medium (100U/mL penicillin/streptomycin) was added and replaced every 3 days. Organoids were grown at 37ºC with 5% CO_2 and passaged according to the manufacturer's instructions. Freshly sorted intestinal ILC3 were added to 5-8 days old epithelial organoids after plating for 24 hours with or without anti-mouse IL-22 antibody (R&D Systems).

IL-22 agonist administration *in vivo*

150 μg of anti-IL-22 antibody (8E11; gift from Genentech, South San Francisco, CA) or mouse IgG1 isotype control (MOPC-21; Bio X Cell) was administered i.p. to Ret^{MEN2B} mice every 2 days. Animals were analysed 2 weeks after the first administration.

Neurosphere-derived glial cells

Neurosphere-derived glial cells were obtained as previously described[60]. Briefly, total intestines from E14.5 C57BL/6J and *Myd88*$^{-/-}$ mice were digested with collagenase D (0.5mg/mL; Roche) and DNase I (0.1mg/ mL; Roche) in DMEM/F-12, GlutaMAX, supplemented with 1% hepes, streptomycin/penicillin and 0.1% β-mercaptoethanol (Gibco) for approximately 30 minutes at 37°C under gentle agitation. Cells were cultured during 1 week in a CO2 incubator at 37 °C in DMEM/F-12, GlutaMAX™, streptomycin and penicillin and 0.1% β-mercaptoethanol (Gibco) supplemented with B27 (Gibco), EGF (Gibco) and FGF2 (Gibco) 20ng/mL. After 1 week of culture cells were treated with 0.05% trypsin (Gibco), transferred into PDL (Sigma-Aldrich) coated plates and culture in DMEM supplemented with 10% FBS, 1% hepes, glutamine, streptomycin and penicillin and 0.1% β-mercaptoethanol (Gibco) until confluence. Glial cells were activated with TLR2 (5μg/ml) (Pam3CSK4), TLR3 (100μg/ml) (PolyI:C), TLR4 (50ng/ml) (LPS), TLR9 (50μg/ml) (DsDNA-EC) ligands from Invivogen and IL-1β (10ng/mL) (401ML005), IL-18 (50ng/mL) (B002-5), IL-33 (0.1 ng/mL) (3626ML) recombinant proteins from R&D Systems. Cells were also co-cultured with purified ILC3 from WT and *Il1b* deficient mice. IL-22 expression in glial-ILC3 co-cultures upon TLR4 activation was also performed using GDNF (2μg/mL) (AB-212–NA), NRTN (2μg/mL) (AF-387sp) and ARTN (0.3μg/mL) (AF-1085-sp) blocking antibodies. Cells were analysed after 24 hours of co-culture.

Statistics

Results are shown as mean ± SEM. Statistical analysis used Microsoft Excel. Variance was analysed using F-test. Student's t-test was performed on homocedastic populations, and Student's t-test with Welch correction was applied on samples with different variances. Analysis of survival curves was performed using a MAntel-Cox test. Results were considered significant at *p 0.05; **p 0.01. Statistical treatment of metagenomics analysis is described in the methods section: 16S rRNA gene sequencing and analysis.
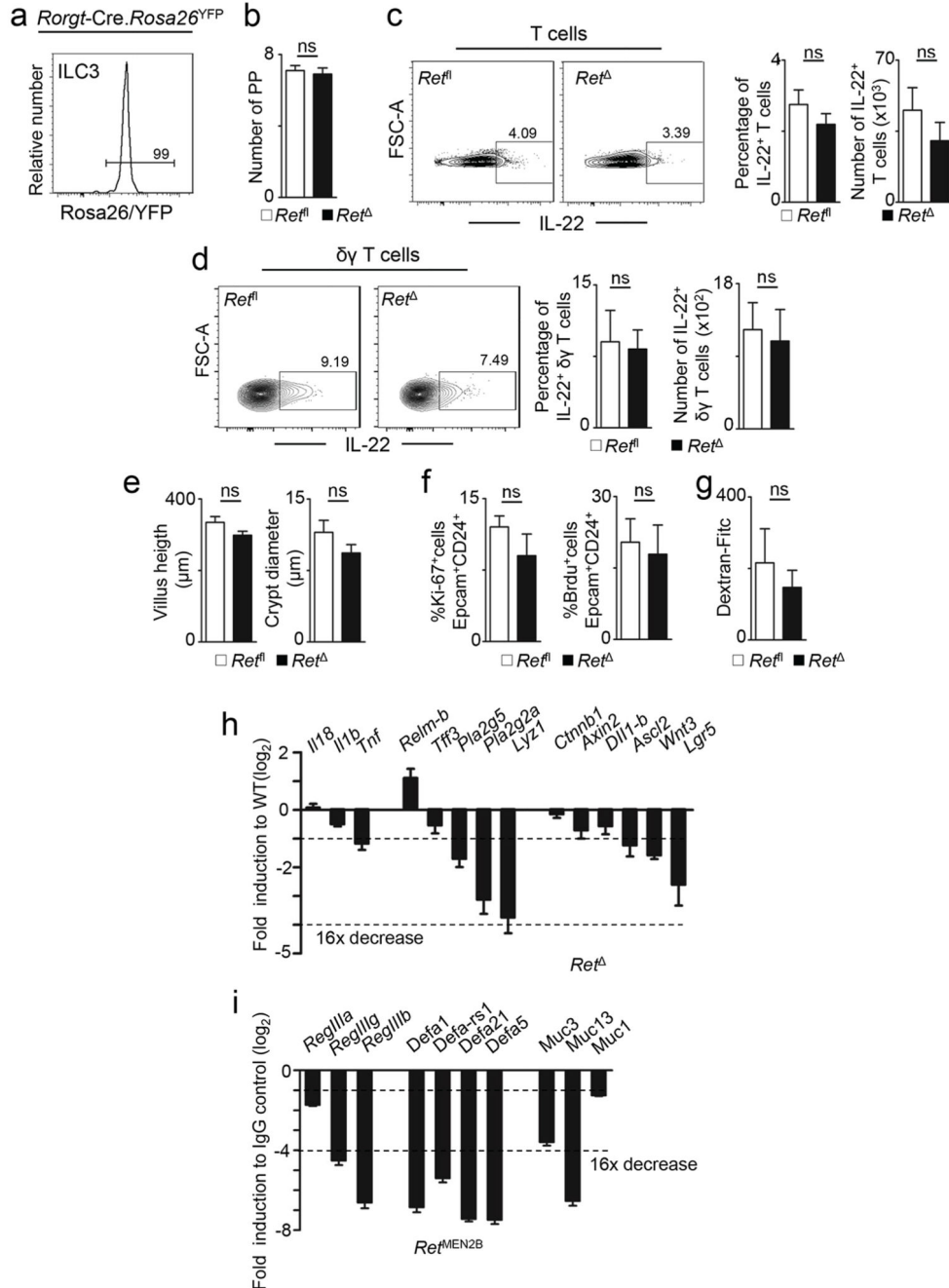
Extended Data
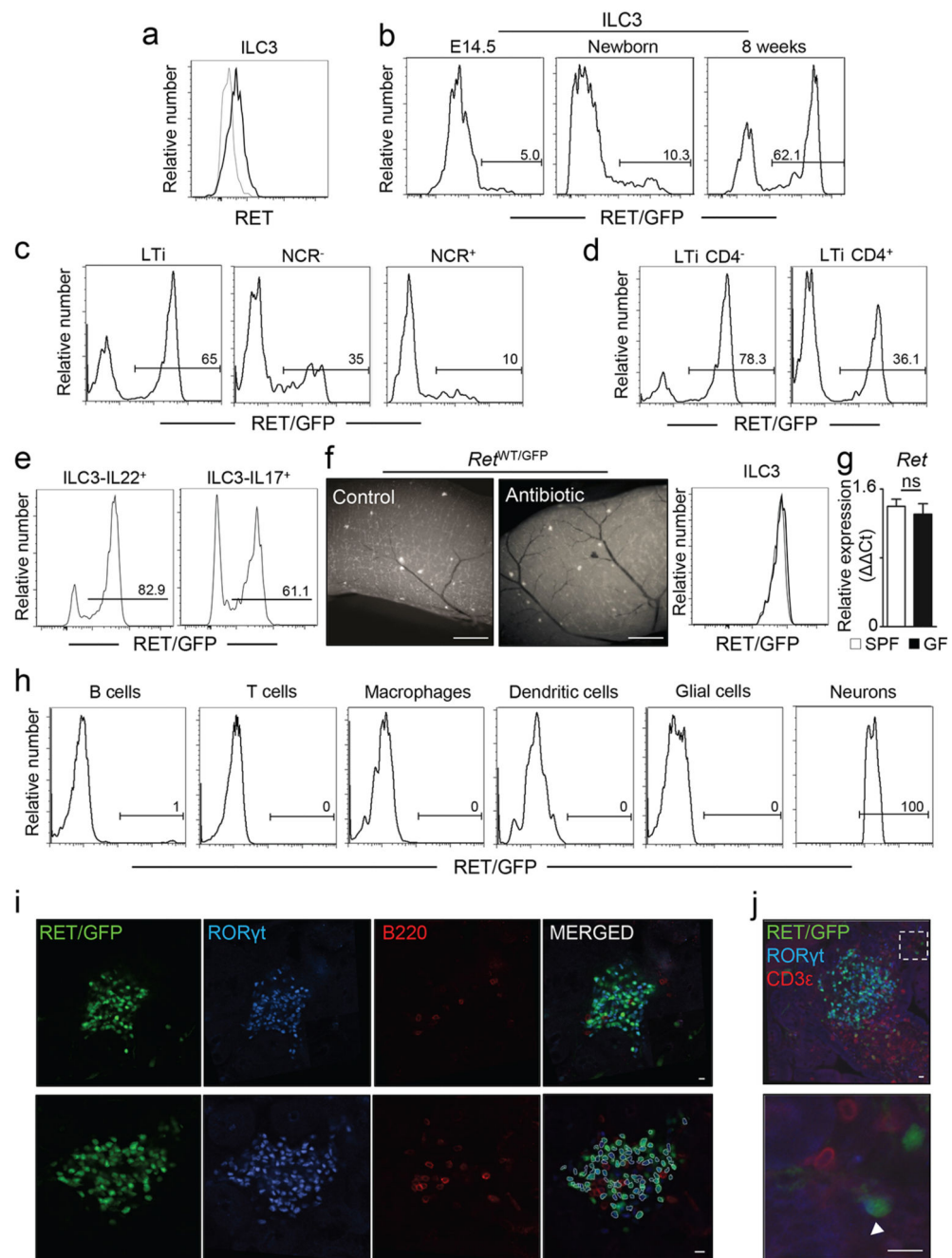
Extended Data Figure 1. ILC3 selectively express the neurotrophic factor receptor RET.
a, Expression of RET protein in gut CD45$^+$Lin$^-$Thy1.2^{hi}IL7Rα$^+$RORγt$^+$ ILC3. **b**, Analysis of gut ILC3 from *Ret*^{GFP} mice. Embryonic day 14.5 (E14.5). **c,d** Analysis of enteric ILC3 subsets from *Ret*^{GFP} mice. **e**, Analysis of cytokine producing ILC3 from *Ret*^{GFP} mice. **f**, Pregnant *Ret*^{GFP} mice were provided with antibiotic cocktails that were maintained after birth until analysis at 6 weeks of age. Left: RET/GFP (white). Right: flow cytometry

analysis of RET/GFP expression in ILC3. Thin line: Ab treated; Bold line: SPF. **g**, *Ret* expression in enteric ILC3 from Germ-Free (GF) mice and Specific Pathogen Free (SPF) controls. n=4. **h**, Analysis of lamina propria populations from *Ret*GFP mice. **i**, Enteric ILC3 clusters. Green: RET/GFP; Blue: RORγt; Red: B220. Bottom: quantification analysis for RET/GFP and RORγt co-expression (79,97 ±4,72%). **j**, Rare RET expressing ILC3 in intestinal villi. Green: RET/GFP; Blue: RORγt; Red: CD3ε. Scale bars: 10μm. Data are representative of 4 independent experiments. Error bars show s.e.m. ns not significant.
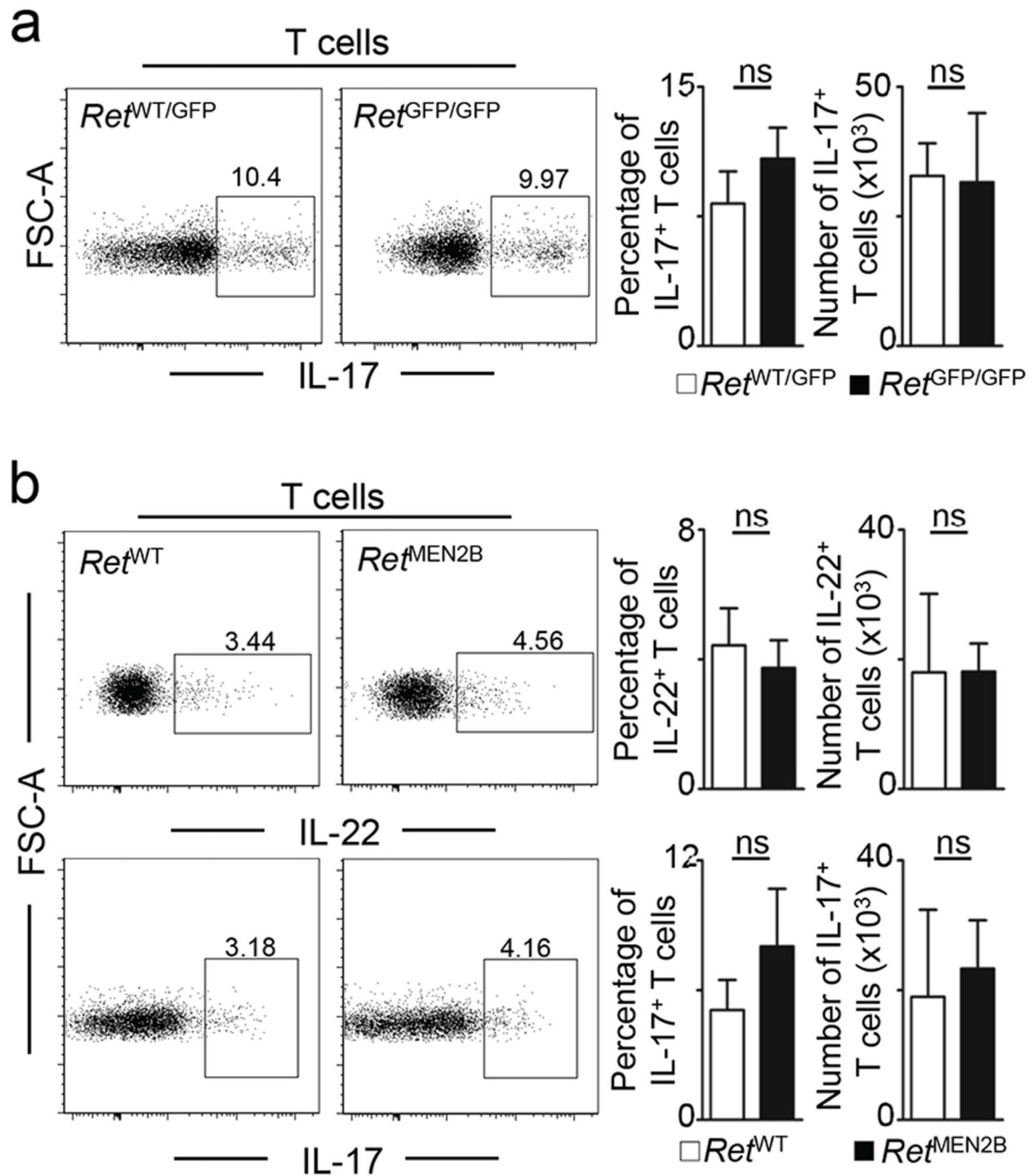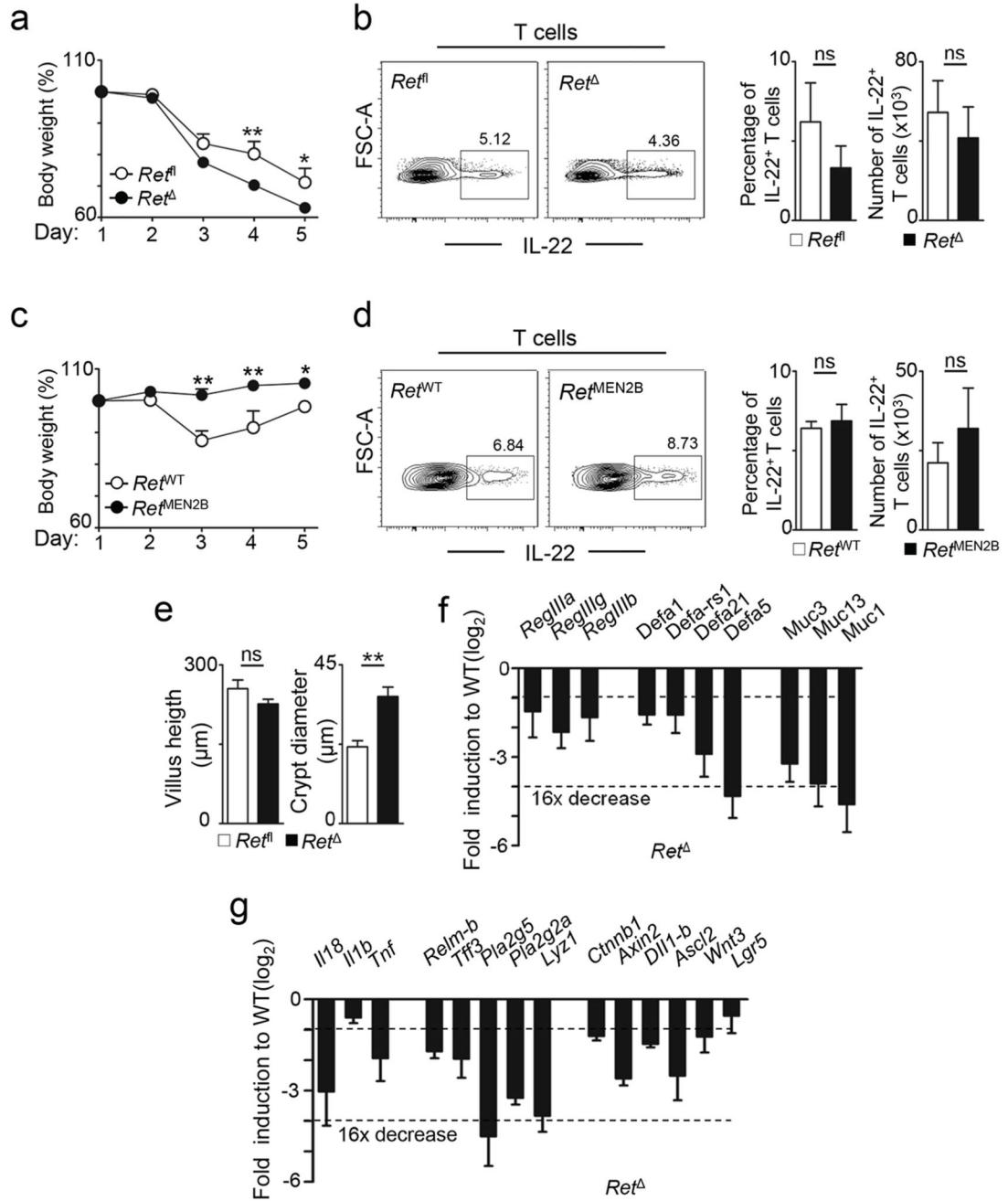
Extended Data Figure 2. T cell-derived IL-22 and IL-17 in *Ret*^GFP chimeras and *Ret*^MEN2B mice.

a, T cell derived IL-17 in *Ret*^GFP chimeras. *Ret*^WT/GFP n=25; *Ret*^GFP/GFP n=22. **b**, T cell derived IL-22 and IL17 in the intestine of *Ret*^MEN2B mice and their WT littermate controls. *Ret*^WT n=7; *Ret*^MEN2B n=7. Data are representative of 4 independent experiments. Error bars show s.e.m. ns not significant.

Extended Data Figure 3. Enteric homeostasis in steady-state *Ret* mice.

a, *Rorgt*-Cre mice were bread to *Rosa26*^{YFP}. Analysis of Rosa26/YFP expression in gut ILC3 from *Rorgt*-Cre.*Rosa26*^{YFP} mice. **b**, Number of Peyer's patches (PP). *Ret*^{fl} n=10; *Ret* n=10. **c**, T cell derived IL-22 in *Ret* mice and their WT littermate controls. *Ret*^{fl} n=11; *Ret* n=11. **d**, γδ T cell derived IL-22 in *Ret* mice and their WT littermate controls. *Ret*^{fl} n=4; *Ret* n=4. **e**, Intestinal villus and crypt morphology. *Ret*^{fl} n=6; *Ret* n=6. **f**, Epithelial cell proliferation. *Ret*^{fl} n=5; *Ret* n=5. **g**, Intestinal paracellular permeability measured by Dextran-Fitc in the plasma. *Ret*^{fl} n=5; *Ret* n=5. **h**, Tissue repair genes in *Ret* intestinal epithelium in comparison to their WT littermate controls. n=8. **i**, Reactivity genes in *Ret*^{MEN2B} mice treated with anti-IL-22 blocking antibodies in comparison to *Ret*^{MEN2B} intestinal epithelium. *Ret*^{MEN2B} n=4; *Ret*^{MEN2B} + anti-IL-22 n=4. Data are representative of 3 independent experiments. Error bars show s.e.m. ns not significant.

Extended Data Figure 4. Enteric inflammation in mice with altered RET signals.
Mice were treated with DSS in the drinking water. **a**, Weight loss of DSS treated *Ret*$^\Delta$ mice and their littermate controls. *Ret*^{fl} n=8; *Ret*$^\Delta$ n=8. **b**, T cell derived IL-22 in *Ret*$^\Delta$ mice and their WT littermate controls after DSS treatment. *Ret*^{fl} n=8; *Ret*$^\Delta$ n=8. **c**, Weight loss of DSS treated *Ret*^{MEN2B} mice and their WT littermate controls. *Ret*^{WT} n=8; *Ret*^{MEN2B} n=8. **d**, T cell derived IL-22 in *Ret*^{MEN2B} mice and their WT littermate controls. *Ret*^{WT} n=8; *Ret*^{MEN2B} n=8. **e**, Intestinal villi and crypt morphology. *Ret*^{fl} n=6; *Ret*$^\Delta$ n=6. **f**, Epithelial reactivity gene expression in DSS treated *Ret*$^\Delta$ mice in comparison to their WT littermate

controls. n=8. **g**, Tissue repair gene expression in DSS treated *Ret* mice in comparison to their WT littermate controls. n=4. Data are representative of 3-4 independent experiments. Error bars show s.e.m. ns not significant. Error bars show s.e.m. *P<0.05; **P<0.01; ns not significant.
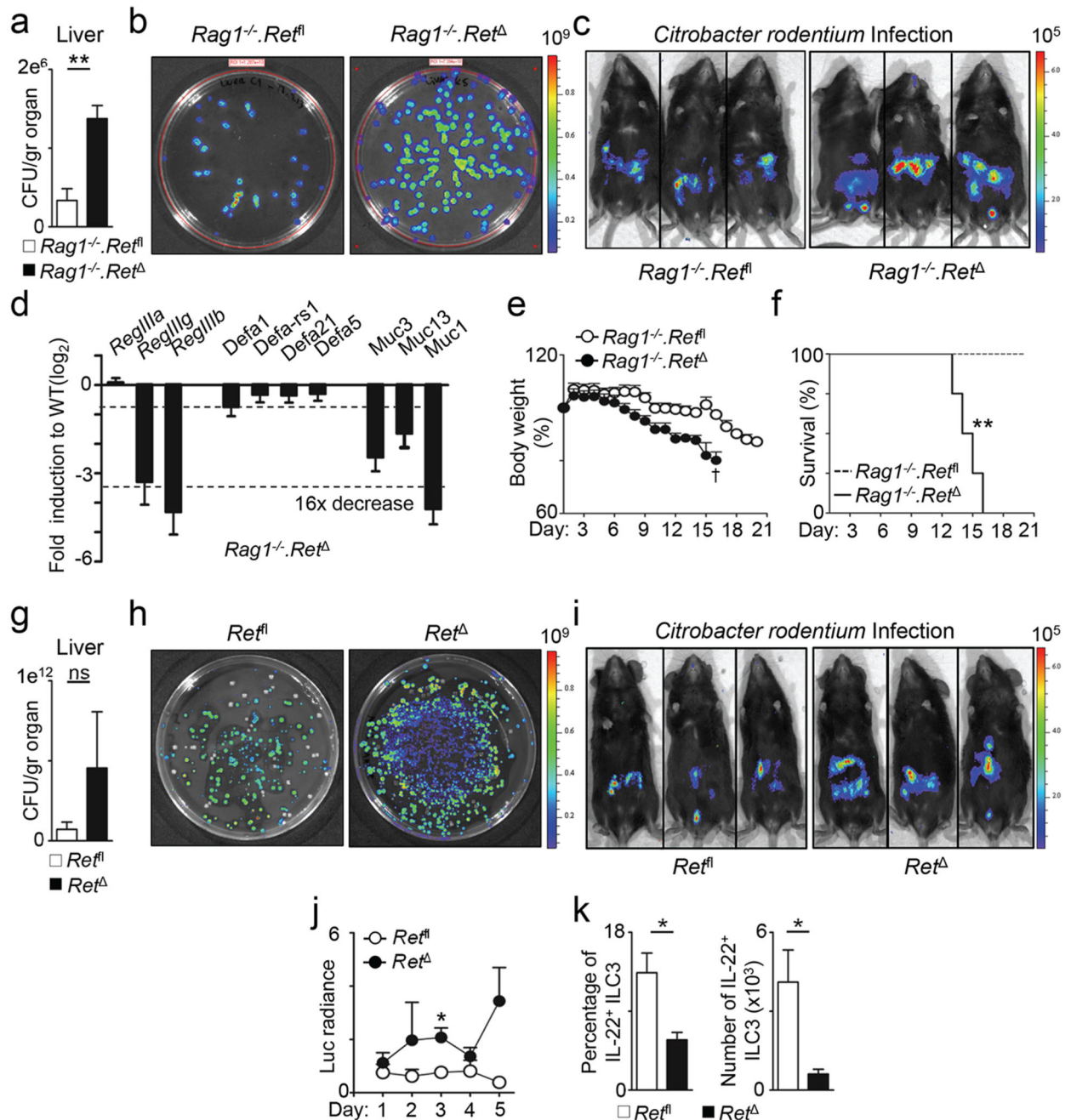
**Extended Data Figure 5.** *Citrobacter rodentium infection in Ret mice.*
a, *C. rodentium* translocation to the liver of *Rag1^-/-.Ret* and their *Rag1^-/-.Ret^fl* littermate controls at day 6 post-infection. n=15. **b**, MacConkey plates of liver cell suspensions from

Rag1^{-/-}.*Ret* and their *Rag1*^{-/-}.*Ret*[fl] littermate controls at day 6 after *C. rodentium* infection. **c**, Whole-body imaging of *Rag1*^{-/-}.*Ret* and their *Rag1*^{-/-}.*Ret*[fl] littermate controls at day 6 after luciferase-expressing *C. rodentium* infection. **d**, Epithelial reactivity gene expression in *C. rodentium* infected *Rag1*^{-/-}.*Ret* mice and their *Rag1*^{-/-}.*Ret*[fl] littermate controls. *Rag1*^{-/-}.*Ret*[fl] n=15; *Rag1*^{-/-}.*Ret* n=17. **e**, Weight loss in *C. rodentium* infected *Rag1*^{-/-}.*Ret* mice and their *Rag1*^{-/-}.*Ret*[fl] littermate controls. *Rag1*^{-/-}.*Ret*[fl] n=8; *Rag1*^{-/-}.*Ret* n=8. **f**, Survival curves in *C. rodentium* infected *Rag1*^{-/-}.*Ret* mice and their *Rag1*^{-/-}.*Ret*[fl] littermate controls. *Rag1*^{-/-}.*Ret*[fl] n=8; *Rag1*^{-/-}.*Ret* n=8. **g**, *C. rodentium* translocation to the liver of *Ret* and their *Ret*[fl] littermate controls at day 6 post-infection. n=6. **h**, MacConkey plates of liver cell suspensions from *Ret* and their *Ret*[fl] littermate controls at day 6 after *C. rodentium* infection. **i**, Whole-body imaging of *Ret* and their *Ret*[fl] littermate controls at day 6 after luciferase-expressing *C. rodentium* infection. **j**, *C. rodentium* infection burden. *Ret*[fl] n=8; *Ret* n=8. **k**, Innate IL-22 in in *C. rodentium* infected *Ret* mice and their *Ret*[fl] littermate controls. *Ret*[fl] n=8; *Ret* n=8. Data are representative of 3-4 independent experiments. Error bars show s.e.m. ns not significant. Error bars show s.e.m. *P<0.05; **P<0.01; ns not significant.
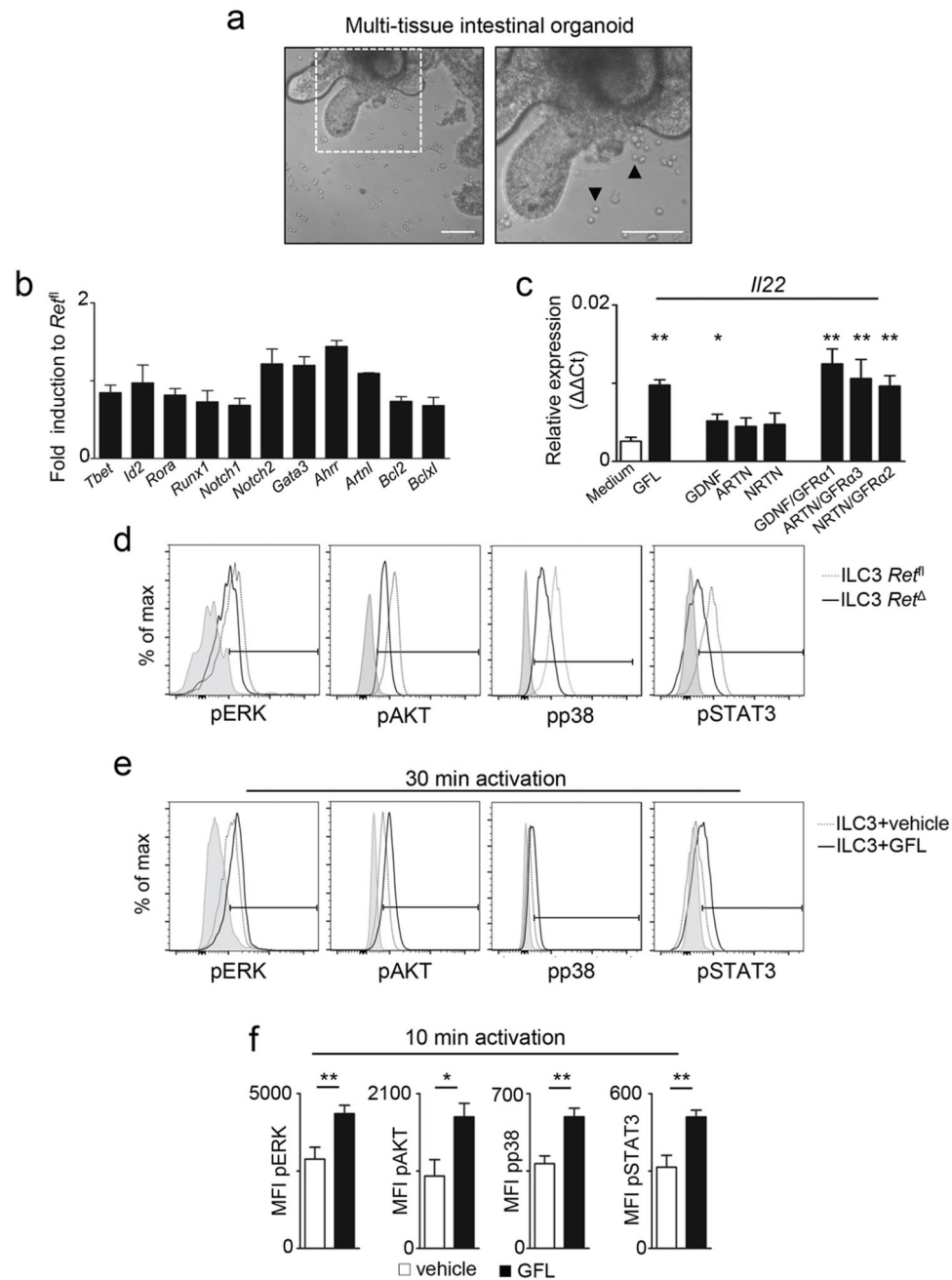
Extended Data Figure 6. Glial-derived neurotrophic factor family ligand (GFL) signals in ILC3.
a, Multi-tissue intestinal organoid system. Scale bar: 20μm. Black arrows: ILC3. **b,** Expression of ILC-related genes in ILC3 from *Ret* mice in comparison to their littermate controls. n=4. **c**, ILC3 activation with all GFL/GFRα pairs (GFL); single GDNF family ligand (GDNF, ARTN or NRTN); or single GFL/GFRα pairs (GDNF/GFRα1, ARTN/GFRα3 or NRTN/GFRα2) compared to vehicle BSA. n=5. **d**, ILC3 from *Ret* mice (open black) and their littermate controls (open dash). Isotype (closed grey). **e**, 30 minutes activation of ILC3 by GFL (open black) compared to vehicle BSA (open dash). Isotype

(closed grey). **f**, 10 minutes activation of ILC3 by GFL. pERK n=8; pAKT n=8; phosphorylated p38/MAP kinase n=8; pSTAT3 n=8. Similar results were obtained in at least 3-4 independent experiments. Error bars show s.e.m. *P<0.05; **P<0.01; ns not significant.
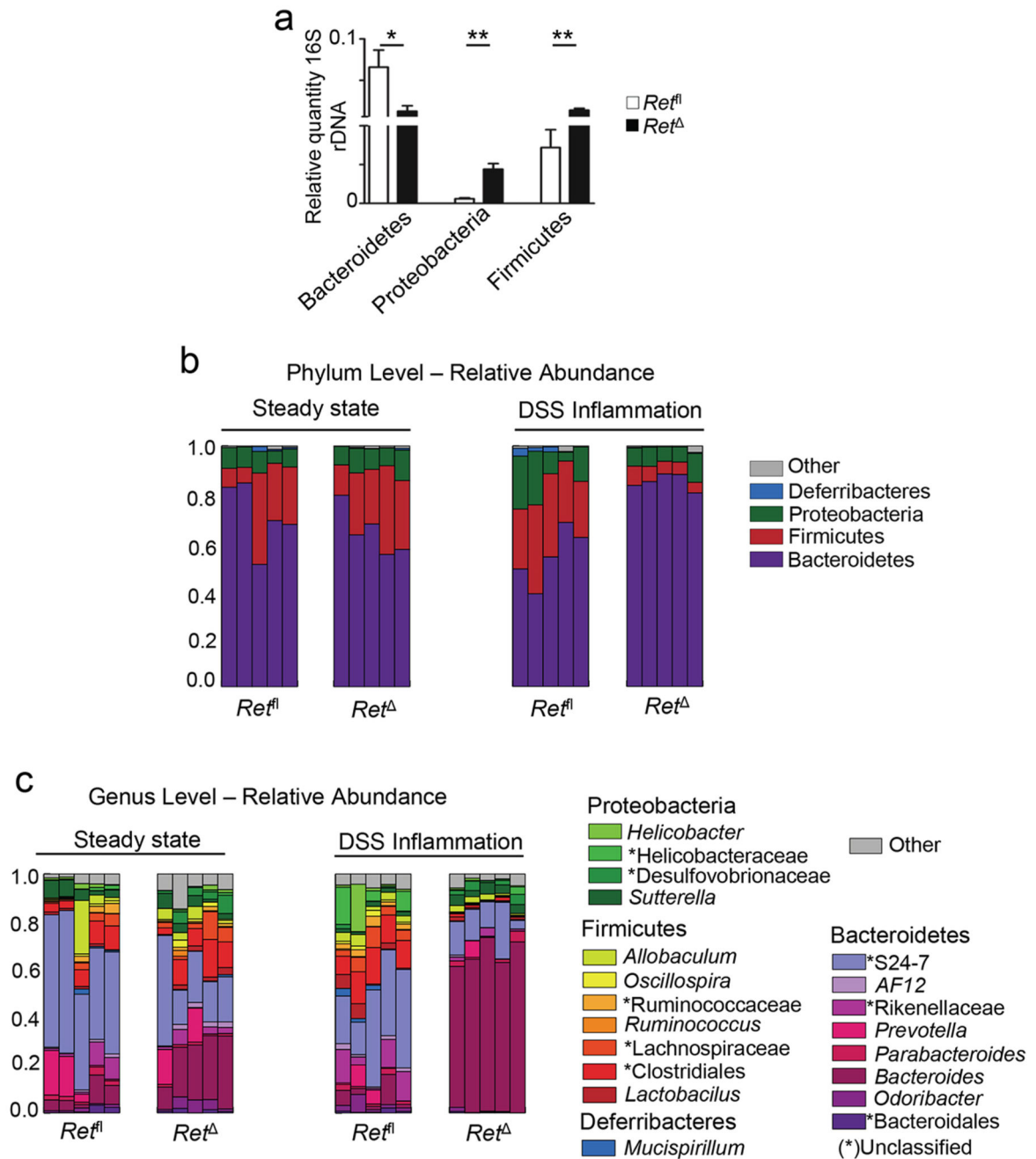
Extended Data Figure 7. Alterations in the diversity of intestinal commensal bacteria of *Ret* mice.

a, Quantitative PCR analysis at the Phylum level in stool bacterial from co-housed *Ret*[fl] and *Ret* littermates in steady state. n=5. **b**, Metagenomic Phylum level comparisons in stool bacterial from co-housed *Ret*[fl] and *Ret* littermates in steady state (left) and after DSS

treatment (right). n=5. **c**, Genus level comparisons in stool bacterial from co-housed Ret^{fl} and $Ret^{}$ littermates in steady state (left) and after DSS treatment (right). n=5. Error bars show s.e.m. *P<0.05; **P<0.01; ns not significant.
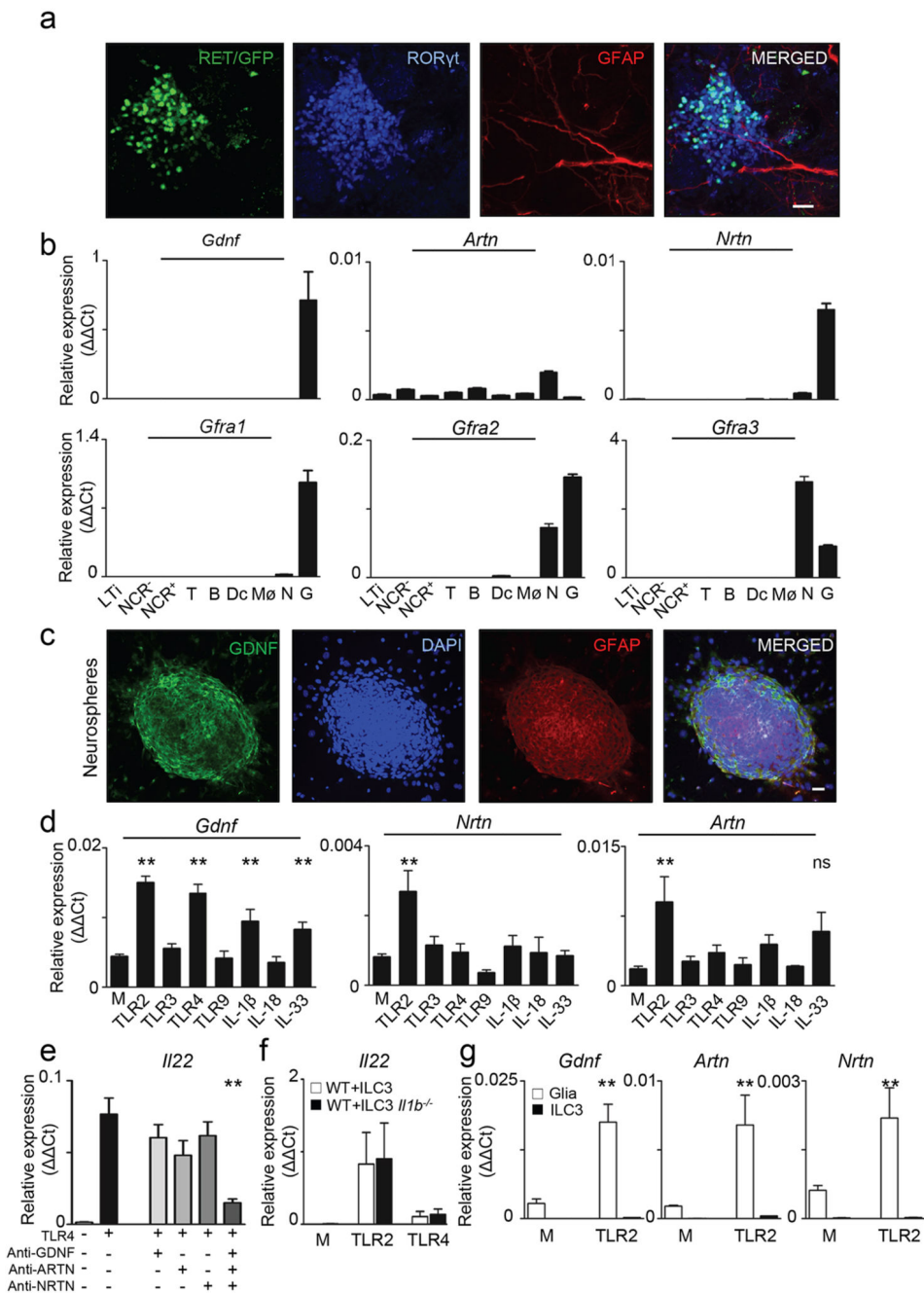
Extended Data Figure 8. GFL expressing glial cells anatomically co-localise with ILC3.
**a,** Intestine of Ret^{GFP} mice. Green: RET/GFP; Red: GFAP; Blue: RORγt. Similar results were obtained in three independent experiments. **b**, Purified lamina propria LTi, NCR⁻ and NCR⁺ ILC3 subsets, T cells (T), B cells (B), Dendritic cells (Dc), Macrophages (Mø),

enteric Neurons (N) and mucosal Glial cells (G). **c**, Neurosphere-derived glial cells. **d**, M: medium. Activation of neurosphere-derived glial cells with TLR2 (Pam3CSK4), TLR3 (Poli I:C), TLR4 (LPS) and TLR9 (DsDNA-EC) ligands, as well as IL-1β, IL-18 and IL-33. n=6. **e**, *Il22* in co-cultures of glial and ILC3 using single or combined GFL antagonists. n=6. **f**, *Il22* in co-cultures of ILC3 and glial cells from *Il1b*^{-/-} or their WT controls. n=3. **g**, *Gdnf, Artn* and *Nrtn* expression in glial cells and ILC3 upon TLR2 stimulation. n=3. Scale bar: 30μm.Similar results were obtained in at least 4 independent experiments.
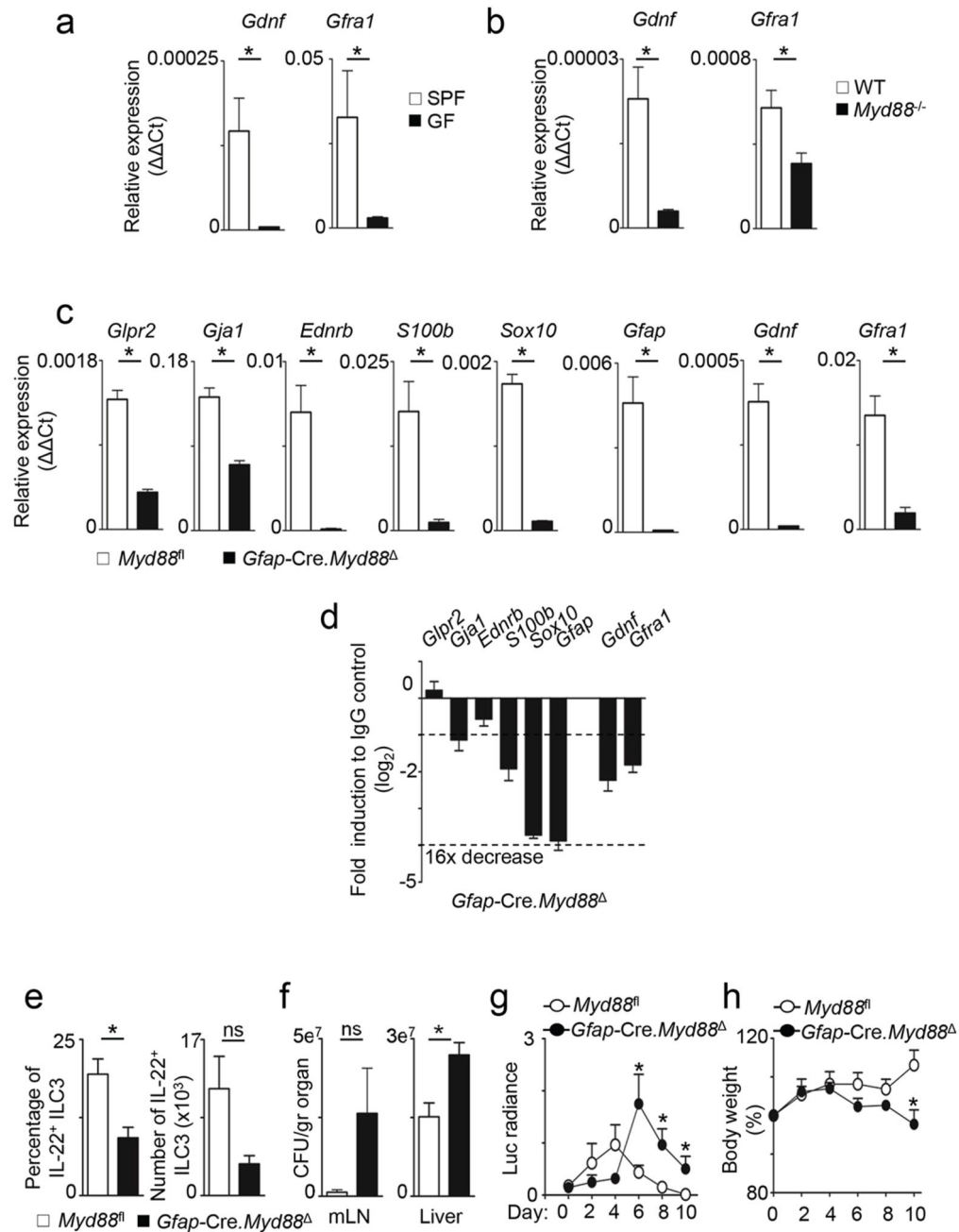
Extended Data Figure 9. Glial cell sensing via MYD88 signals.
a-c, Intestinal glial cells were purified by flow cytometry. **a**, Germ-free (GF) and their respective Specific Pathogen Free (SPF) controls. n=3. **b**, Myd88$^{-/-}$ and their respective WT littermate controls. n=3. **c**, *Gfap*-Cre.*Myd88* and their littermate controls (*Myd88*^{fl}). n=3. **d**, Total lamina propria cells of *Gfap*-Cre.*Myd88* and their littermate controls (*Myd88*^{fl}). n=6. **e-h**, *Citrobacter rodentium* infection of *Gfap*-Cre.*Myd88* mice and their littermate controls (*Myd88*^{fl}). n=6. **e**, Innate IL-22. **f**, *Citrobacter rodentium* translocation. **g**, Infection burden. **h**, Weight loss. Data are representative of 3 independent experiments. Error bars show s.e.m. *P<0.05; **P<0.01; ns not significant.
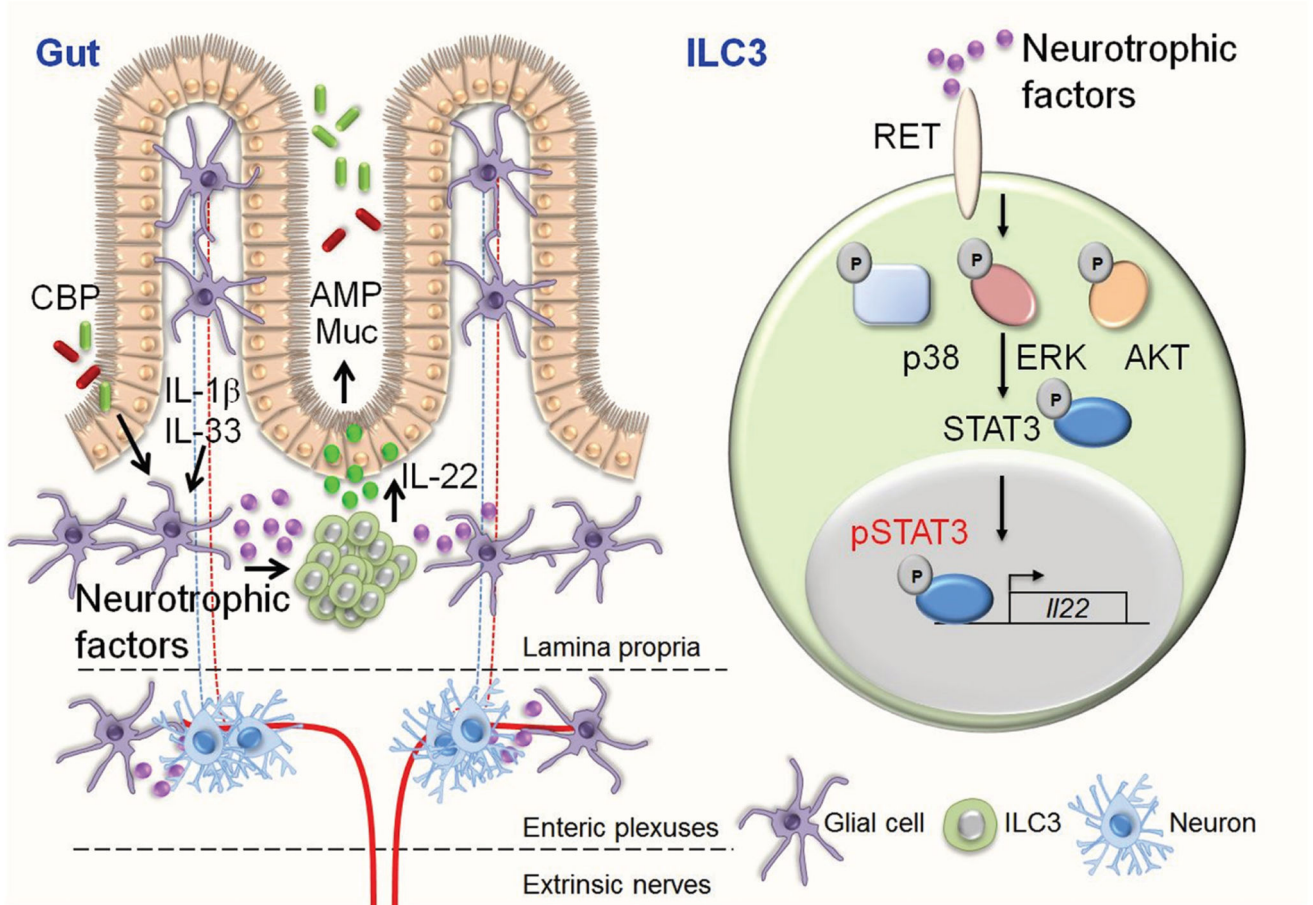
Extended Data Figure 10. A novel glial-ILC3-epithelial cell unit orchestrated by neurotrophic factors.
Lamina propria glial cells sense microenvironmental products, that control neurotrophic factor expression. Glial-derived neurotrophic factors operate in an ILC3-intrinsic manner by activating the tyrosine kinase RET, which directly regulates innate IL-22 downstream of a p38 MAPK/ERK-AKT cascade and STAT3 phosphorylation. GFL induced innate IL-22 acts on epithelial cells to induce reactivity gene expression (CBP: Commensal bacterial products; AMP: antimicrobial peptides; Muc: mucins). Thus, neurotrophic factors are the molecular link between glial cell sensing, innate IL-22 production and intestinal epithelial barrier defence.

Acknowledgements

## References

1. Artis D, Spits H. The biology of innate lymphoid cells. Nature. 2015; 517:293–301. [PubMed: 25592534]

2. van de Pavert SA, et al. Maternal retinoids control type 3 innate lymphoid cells and set the offspring immunity. Nature. 2014; 508:123–127. [PubMed: 24670648]

3. Spencer SP, et al. Adaptation of innate lymphoid cells to a micronutrient deficiency promotes type 2 barrier immunity. Science. 2014; 343:432–437. [PubMed: 24458645]

4. Kiss EA, et al. Natural aryl hydrocarbon receptor ligands control organogenesis of intestinal lymphoid follicles. Science. 2011; 334:1561–1565. [PubMed: 22033518]

5. Lee JS, et al. AHR drives the development of gut ILC22 cells and postnatal lymphoid tissues via pathways dependent on and independent of Notch. Nat Immunol. 2011; 13:144–151. [PubMed: 22101730]

6. Qiu J, et al. The aryl hydrocarbon receptor regulates gut immunity through modulation of innate lymphoid cells. Immunity. 2011; 36:92–104. [PubMed: 22177117]

7. Mulligan LM. RET revisited: expanding the oncogenic portfolio. Nat Rev Cancer. 2014; 14:173–186. [PubMed: 24561444]

8. Fonseca-Pereira D, et al. The neurotrophic factor receptor RET drives haematopoietic stem cell survival and function. Nature. 2014; 514:98–101. [PubMed: 25079320]

9. Veiga-Fernandes H, et al. Tyrosine kinase receptor RET is a key regulator of Peyer's Patch organogenesis. Nature. 2007; 446:547–551. [PubMed: 17322904]

10. Patel A, et al. Differential RET signaling pathways drive development of the enteric lymphoid and nervous systems. Sci Signal. 2012; 5:ra55. [PubMed: 22855506]

11. Almeida AR, et al. The neurotrophic factor receptor RET regulates IL-10 production by in vitro polarised T helper 2 cells. Eur J Immunol. 2014; 44:3605–3613. [PubMed: 25168352]

12. Robinette ML, et al. Transcriptional programs define molecular characteristics of innate lymphoid cell classes and subsets. Nat Immunol. 2015; 16:306–317. [PubMed: 25621825]

13. Hoshi M, Batourina E, Mendelsohn C, Jain S. Novel mechanisms of early upper and lower urinary tract patterning regulated by RetY1015 docking tyrosine in mice. Development. 2012; 139:2405–2415. [PubMed: 22627285]

14. Smith-Hicks CL, Sizer KC, Powers JF, Tischler AS, Costantini F. C-cell hyperplasia, pheochromocytoma and sympathoadrenal malformation in a mouse model of multiple endocrine neoplasia type 2B. Embo J. 2000; 19:612–622. [PubMed: 10675330]

15. Sawa S, et al. Lineage relationship analysis of RORgammat+ innate lymphoid cells. Science. 2010; 330:665–669. [PubMed: 20929731]

16. Almeida AR, et al. RET/GFRalpha signals are dispensable for thymic T cell development in vivo. PLoS One. 2012; 7:e52949. [PubMed: 23300832]

17. Rutz S, Wang X, Ouyang W. The IL-20 subfamily of cytokines--from host defence to tissue homeostasis. Nat Rev Immunol. 2014; 14:783–795. [PubMed: 25421700]

18. Xu W, et al. NFIL3 orchestrates the emergence of common helper innate lymphoid cell precursors. Cell Rep. 2015; 10:2043–2054. [PubMed: 25801035]

19. Wen H, et al. ZMYND11 links histone H3.3K36me3 to transcription elongation and tumour suppression. Nature. 2014; 508:263–268. [PubMed: 24590075]

20. Garrett WS, et al. Enterobacteriaceae act in concert with the gut microbiota to induce spontaneous and maternally transmitted colitis. Cell Host Microbe. 2010; 8:292–300. [PubMed: 20833380]

21. Elinav E, et al. NLRP6 inflammasome regulates colonic microbial ecology and risk for colitis. Cell. 2011; 145:745–757. [PubMed: 21565393]

22. Rakoff-Nahoum S, Paglino J, Eslami-Varzaneh F, Edberg S, Medzhitov R. Recognition of commensal microflora by toll-like receptors is required for intestinal homeostasis. Cell. 2004; 118:229–241. [PubMed: 15260992]

23. Neunlist M, et al. The digestive neuronal-glial-epithelial unit: a new actor in gut health and disease. Nature reviews. Gastroenterology & hepatology. 2013; 10:90–100. [PubMed: 23165236]

24. Brun P, et al. Toll-like receptor 2 regulates intestinal inflammation by controlling integrity of the enteric nervous system. Gastroenterology. 2013; 145:1323–1333. [PubMed: 23994200]

25. Kabouridis PS, et al. Microbiota controls the homeostasis of glial cells in the gut lamina propria. Neuron. 2015; 85:289–295. [PubMed: 25578362]

26. Zhuo L, et al. hGFAP-cre transgenic mice for manipulation of glial and neuronal function in vivo. Genesis. 2001; 31:85–94. [PubMed: 11668683]

27. Hou B, Reizis B, DeFranco AL. Toll-like receptors activate innate and adaptive immunity by using dendritic cell-intrinsic and -extrinsic mechanisms. Immunity. 2008; 29:272–282. [PubMed: 18656388]

28. van de Pavert SA, et al. Chemokine CXCL13 is essential for lymph node initiation and is induced by retinoic acid and neuronal stimulation. Nat Immunol. 2009; 10:1193–1199. [PubMed: 19783990]

29. Bush TG, et al. Fulminant jejuno-ileitis following ablation of enteric glia in adult transgenic mice. Cell. 1998; 93:189–201. [PubMed: 9568712]

30. Veiga-Fernandes H, Mucida D. Neuro-Immune Interactions at Barrier Surfaces. Cell. 2016; 165:801–811. [PubMed: 27153494]

31. Cao X, et al. Defective lymphoid development in mice lacking expression of the common cytokine receptor gamma chain. Immunity. 1995; 2:223–238. [PubMed: 7697543]

32. Mombaerts P, et al. RAG-1-deficient mice have no mature B and T lymphocytes. Cell. 1992; 68:869–877. [PubMed: 1547488]

33. Srinivas S, et al. Cre reporter strains produced by targeted insertion of EYFP and ECFP into the ROSA26 locus. BMC Dev Biol. 2001; 1:4. [PubMed: 11299042]

34. Madisen L, et al. A robust and high-throughput Cre reporting and characterization system for the whole mouse brain. Nature neuroscience. 2010; 13:133–140. [PubMed: 20023653]

35. Horai R, et al. Production of mice deficient in genes for interleukin (IL)-1alpha, IL-1beta, IL-1alpha/beta, and IL-1 receptor antagonist shows that IL-1beta is crucial in turpentine-induced fever development and glucocorticoid secretion. The Journal of experimental medicine. 1998; 187:1463–1475. [PubMed: 9565638]

36. Adachi O, et al. Targeted disruption of the MyD88 gene results in loss of IL-1- and IL-18-mediated function. Immunity. 1998; 9:143–150. [PubMed: 9697844]

37. Wiles S, Pickard KM, Peng K, MacDonald TT, Frankel G. In vivo bioluminescence imaging of the murine pathogen Citrobacter rodentium. Infect Immun. 2006; 74:5391–5396. [PubMed: 16926434]

38. Collins JW, et al. Citrobacter rodentium: infection, inflammation and the microbiota. Nat Rev Microbiol. 2014; 12:612–623. [PubMed: 25088150]

39. Ibiza S, et al. Endothelial nitric oxide synthase regulates T cell receptor signaling at the immunological synapse. Immunity. 2006; 24:753–765. [PubMed: 16782031]

40. Moolenbeek C, Ruitenberg EJ. The Swiss Roll - a Simple Technique for Histological Studies of the Rodent Intestine. Lab Anim. 1981; 15:57–59. [PubMed: 7022018]

41. Burich A, et al. Helicobacter-induced inflammatory bowel disease in IL-10- and T cell-deficient mice. Am J Physiol Gastrointest Liver Physiol. 2001; 281:G764–778. [PubMed: 11518689]

42. Fort MM, et al. A synthetic TLR4 antagonist has anti-inflammatory effects in two murine models of inflammatory bowel disease. J Immunol. 2005; 174:6416–6423. [PubMed: 15879143]

43. Seamons A, Treuting PM, Brabb T, Maggio-Price L. Characterization of dextran sodium sulfate-induced inflammation and colonic tumorigenesis in Smad3(-/-) mice with dysregulated TGFbeta. PLoS One. 2013; 8:e79182. [PubMed: 24244446]

44. Bogunovic M, et al. Origin of the lamina propria dendritic cell network. Immunity. 2009; 31:513–525. [PubMed: 19733489]

45. Muller PA, et al. Crosstalk between muscularis macrophages and enteric neurons regulates gastrointestinal motility. Cell. 2014; 158:300–313. [PubMed: 25036630]

46. Sanos SL, Diefenbach A. Isolation of NK cells and NK-like cells from the intestinal lamina propria. Methods Mol Biol. 2010; 612:505–517. [PubMed: 20033661]

47. Joseph NM, et al. Enteric glia are multipotent in culture but primarily form glia in the adult rodent gut. The Journal of clinical investigation. 2011; 121:3398–3411. [PubMed: 21865643]

48. Escobar TM, et al. miR-155 activates cytokine gene expression in Th17 cells by regulating the DNA-binding protein Jarid2 to relieve polycomb-mediated repression. Immunity. 2014; 40:865–879. [PubMed: 24856900]

49. Guo X, et al. Induction of innate lymphoid cell-derived interleukin-22 by the transcription factor STAT3 mediates protection against intestinal infection. Immunity. 2014; 40:25–39. [PubMed: 24412612]

50. Yeste A, et al. IL-21 induces IL-22 production in CD4+ T cells. Nat Commun. 2014; 5:3753. [PubMed: 24796415]

51. Misic AM, et al. The shared microbiota of humans and companion animals as evaluated from Staphylococcus carriage sites. Microbiome. 2015; 3:2. [PubMed: 25705378]

52. Schloss PD, et al. Introducing mothur: open-source, platform-independent, community-supported software for describing and comparing microbial communities. Appl Environ Microbiol. 2009; 75:7537–7541. [PubMed: 19801464]

53. Caporaso JG, et al. QIIME allows analysis of high-throughput community sequencing data. Nature methods. 2010; 7:335–336. [PubMed: 20383131]

54. Haas BJ, et al. Chimeric 16S rRNA sequence formation and detection in Sanger and 454-pyrosequenced PCR amplicons. Genome Res. 2011; 21:494–504. [PubMed: 21212162]

55. Fu L, Niu B, Zhu Z, Wu S, Li W. CD-HIT: accelerated for clustering the next-generation sequencing data. Bioinformatics. 2012; 28:3150–3152. [PubMed: 23060610]

56. Wang Q, Garrity GM, Tiedje JM, Cole JR. Naive Bayesian classifier for rapid assignment of rRNA sequences into the new bacterial taxonomy. Appl Environ Microbiol. 2007; 73:5261–5267. [PubMed: 17586664]

57. Caporaso JG, et al. PyNAST: a flexible tool for aligning sequences to a template alignment. Bioinformatics. 2010; 26:266–267. [PubMed: 19914921]

58. Price MN, Dehal PS, Arkin AP. FastTree: computing large minimum evolution trees with profiles instead of a distance matrix. Mol Biol Evol. 2009; 26:1641–1650. [PubMed: 19377059]

59. Lozupone C, Hamady M, Knight R. UniFrac--an online tool for comparing microbial community diversity in a phylogenetic context. BMC Bioinformatics. 2006; 7:371. [PubMed: 16893466]

60. Mich JK, et al. Prospective identification of functionally distinct stem cells and neurosphere-initiating cells in adult mouse forebrain. eLife. 2014; 3:e02669. [PubMed: 24843006]
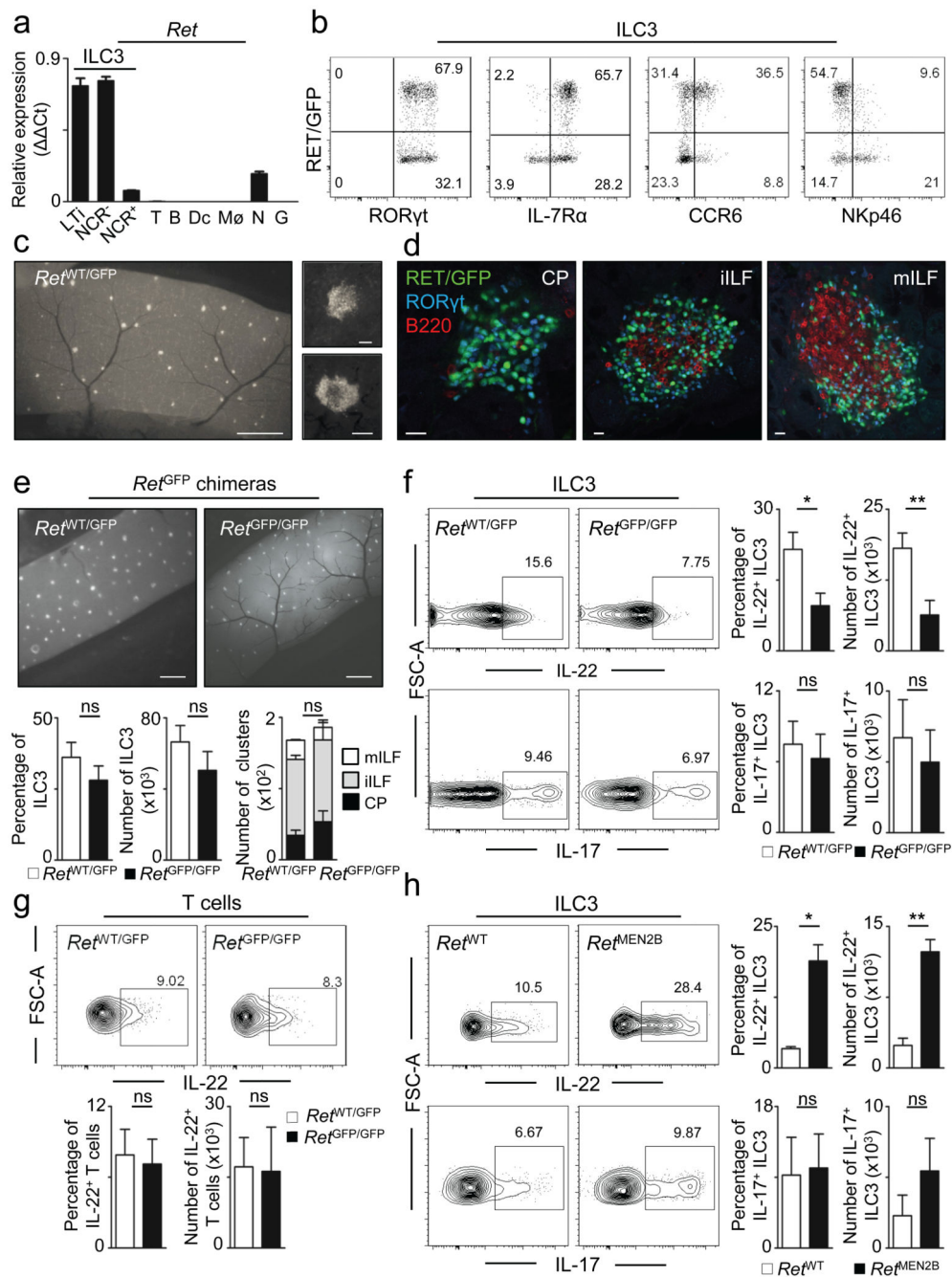
Figure 1. The neurotrophic factor receptor RET drives enteric ILC3-derived IL-22.
a, LTi, NCR⁻ and NCR⁺ ILC3 subsets, T cells (T), B cells (B), Dendritic cells (Dc), Macrophages (Mø), enteric Neurons (N) and mucosal Glial cells (G). **b**, *Ret*GFP ILC3. **c**, Left: *Ret*GFP gut. White: GFP. Right: ILC3 aggregates. **d**, Cryptopatches (CP), immature (iILF) and mature (mILF) isolated lymphoid follicles. Green: RET/GFP; Blue: RORγt; Red: B220. **e**, *Ret*GFP chimeras. n=15. **f,g**, *Ret*GFP chimeras. *Ret*WT/GFP n=25; *Ret*GFP/GFP n=22. **h**, *Ret*MEN2B mice. n=7. Scale bars: 1mm (c left, e); 50μm (c right); 30μm (d). Data are

representative of 4 independent experiments. Error bars show s.e.m. *P<0.05; **P<0.01; ns not significant.
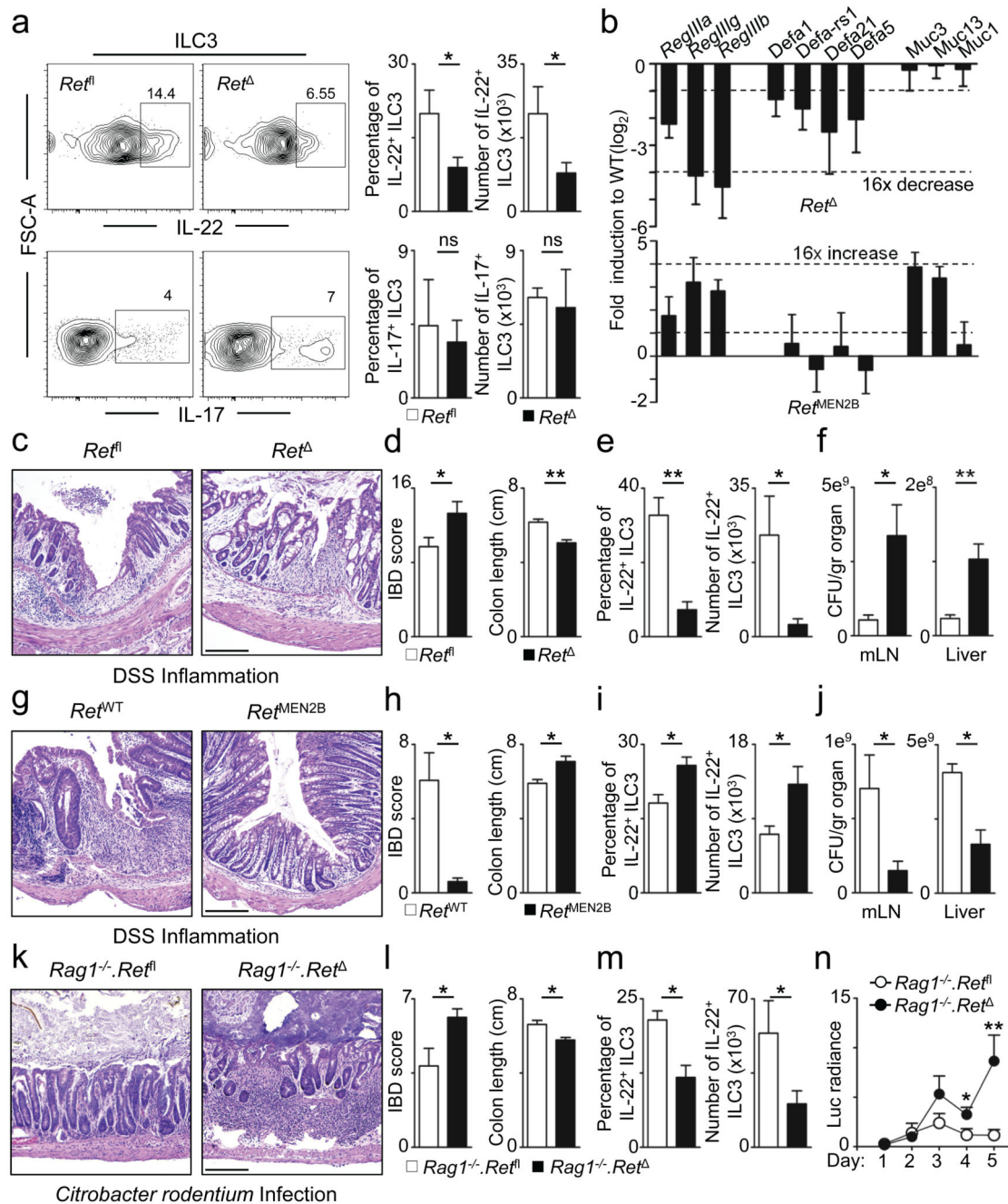
Figure 2. ILC3-intrinsic RET signals regulate gut defence.
a, ILC3-derived cytokines. n=11. **b**, Ret^{Δ} and Ret^{MEN2B} mice compared to their WT littermate controls. n=7. **c-f**, DSS treatment. Ret^{fl} n=8; Ret^{Δ} n=8. **c**, Histopathology. **d**, Inflammation score and colon length. **e**, Innate IL-22. **f**, Bacterial translocation. **g-j**, DSS treatment. Ret^{WT} n=8; Ret^{MEN2B} n=8. **g**, Histopathology. **h**, Inflammation score and colon length. **i**, Innate IL-22. **j**, Bacterial translocation. **k-n**, $C.\ rodentium$ infection. $Rag1^{-/-}.Ret^{fl}$ n=15; $Rag1^{-/-}.Ret^{\Delta}$ n=17. **k**, Histopathology. **l**, Inflammation score and colon length. **m**,

Innate IL-22. **n**, Infection burden. Scale bars: 200μm. Data are representative of 4 independent experiments. Error bars show s.e.m. *P<0.05; **P<0.01; ns not significant.
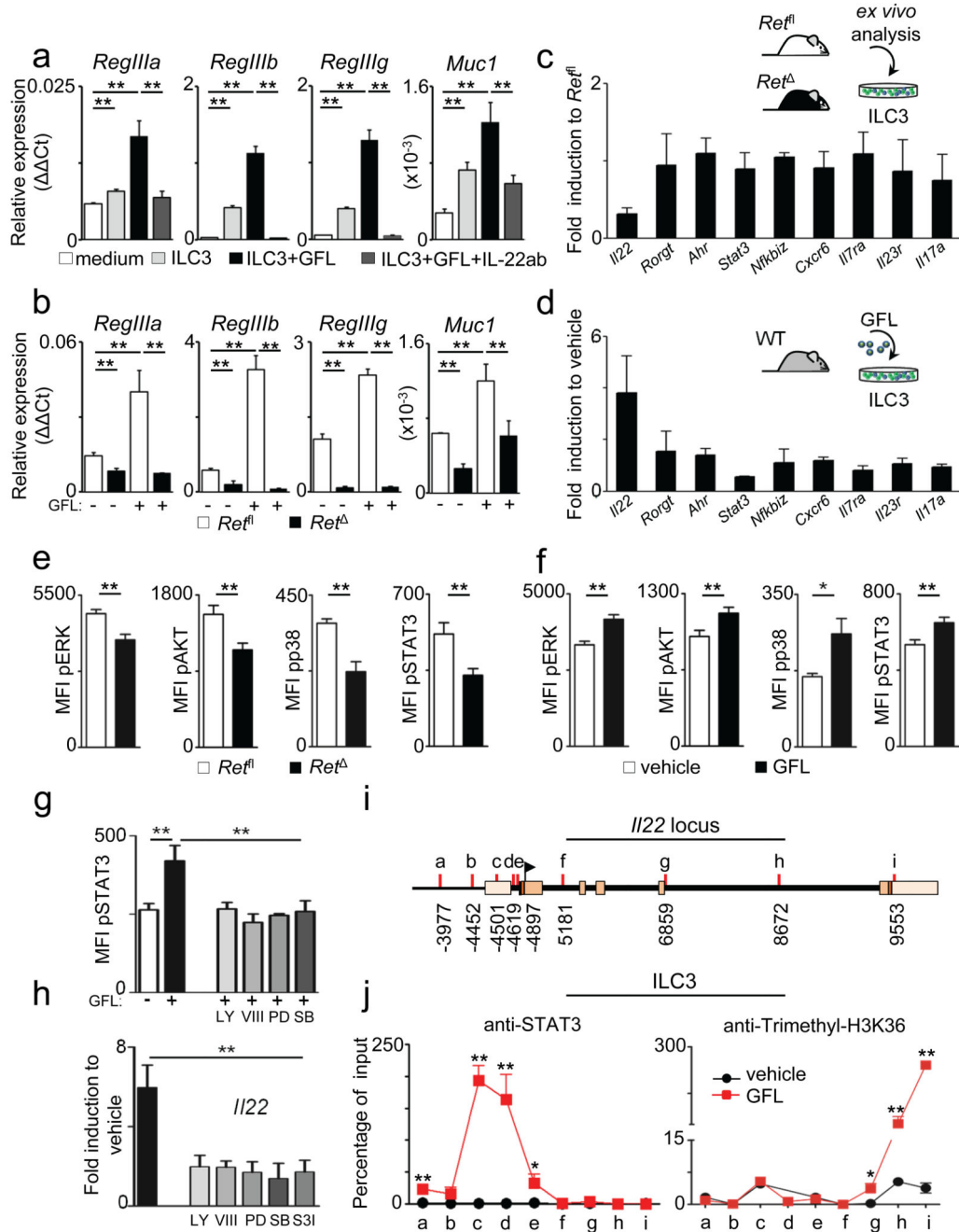
Figure 3. ILC3-autonomous RET signals directly control *Il22* downstream of pSTAT3.
a,b, Epithelial/ILC3 organoids. n=9. **c**, *Ret* ILC3 compared to their WT controls. n=4. **d**, ILC3 activation by GFL. n=4. **e**, *Ret* ILC3. pERK n=8; pAKT n=12; phosphorylated p38/MAP kinase n=6; pSTAT3 n=14. **f**, ILC3 activation by GFL. pERK n=10; pAKT n=16; phosphorylated p38/MAP kinase n=3; pSTAT3 n=15. **g**, pSTAT3 in ILC3 cultured with medium (n=7), GFL (n=11) or GFL and inhibitors for: p38 MAPK/ERK-AKT (LY) (n=7); ERK (PD) (n=7); AKT (VIII) (n=8); and p38 MAPK (SB) (n=6). **h**, *Il22* in ILC3 cultured with GFL (n=17) or GFL and the inhibitors LY (n=18); PD (n=16); VIII (n=15); SB (n=15);

and the STAT3 inhibitor (S3I) (n=8). **i**, *Il22* locus. **j.** ChIP analysis of ILC3 stimulated with GFL. n=10. Data are representative of 3 independent experiments. Error bars show s.e.m. *P<0.05; **P<0.01; ns not significant.
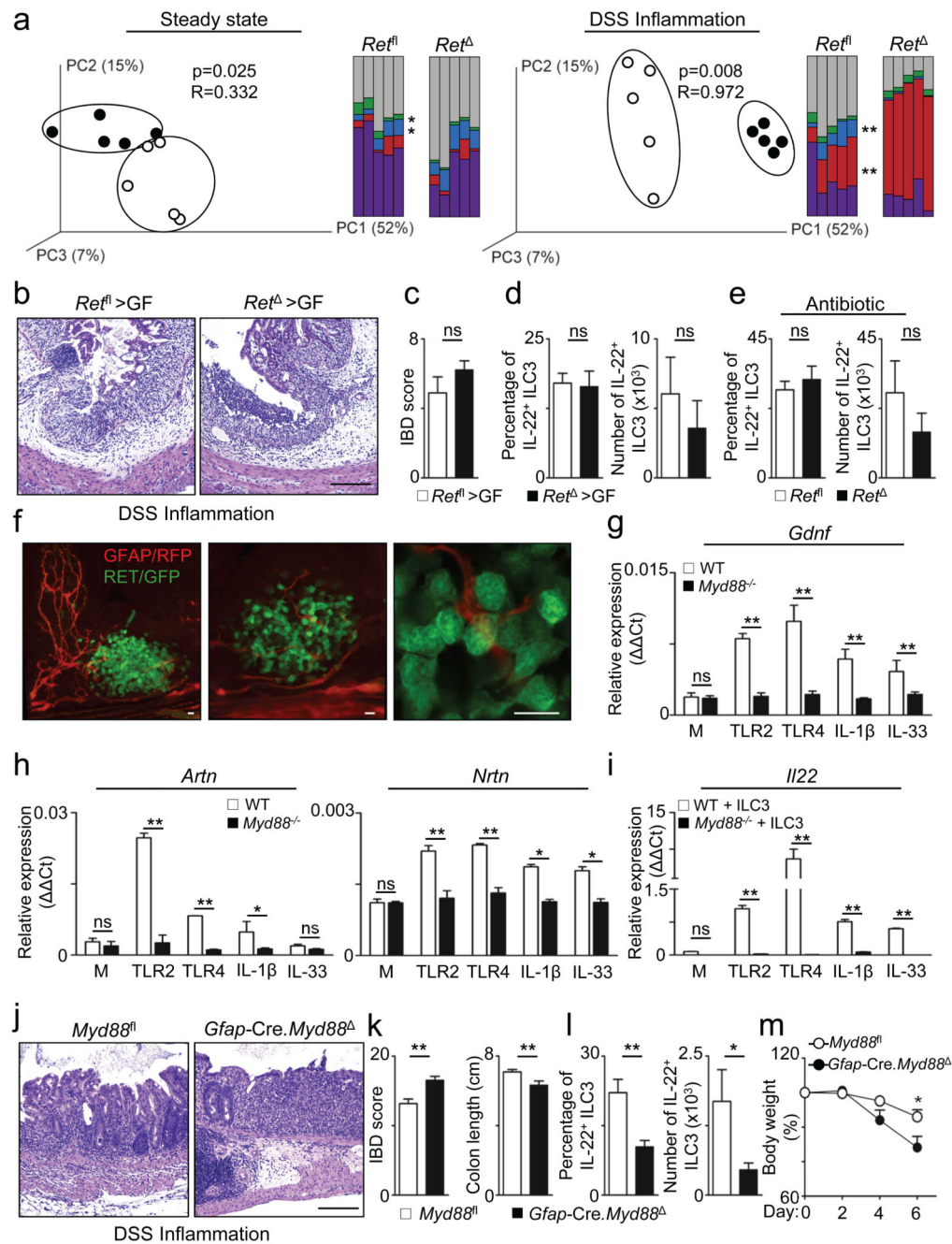
Figure 4. Glial cells set GFL expression and innate IL-22, via MYD88-dependent sensing of the microenvironment.

a, Weighted Unifrac PCoA analysis and genus-level comparisons from co-housed *Ret*^fl (white circles) and *Ret*^Δ (black circles) littermates. n=5. Purple: Unclassified *S24-7*; Red: *Bacteroides*; Green: *Sutterella*; Blue: Unclassified *Clostridiales*; Grey: Other. **b-d**, DSS treatment of colonised germ-free (GF) mice. n=5. **b**, Histopathology. **c**, Inflammation score. **d**, Innate IL-22. **e**, Innate IL-22 after antibiotic treatment. n=8. **f**, *Ret*^GFP.*Gfap*-Cre.*Rosa26*^RFP mice. Green: RET/GFP; Red: GFAP/RFP. **g,h**, Glial cell activation with

TLR2, TLR4, IL-1β receptor and IL-33 receptor ligands. n=6. **i**, TLR ligands, IL-1β and IL-33 activation of co-cultured ILC3 with WT (white bars) or *Myd88*$^{-/-}$ glial cells (black bars). n=6. **j-m**, DSS treatment of *Gfap*-Cre.*Myd88* mice. n=12. **j**, Histopathology. **k**, Inflammation score and colon length. **l**, Innate IL-22. **m**, Body weight. Scale bars: 200μm (b, j); 10μm (f). Data are representative of 3-4 independent experiments. Error bars show s.e.m. *P<0.05; **P<0.01; ns not significant.